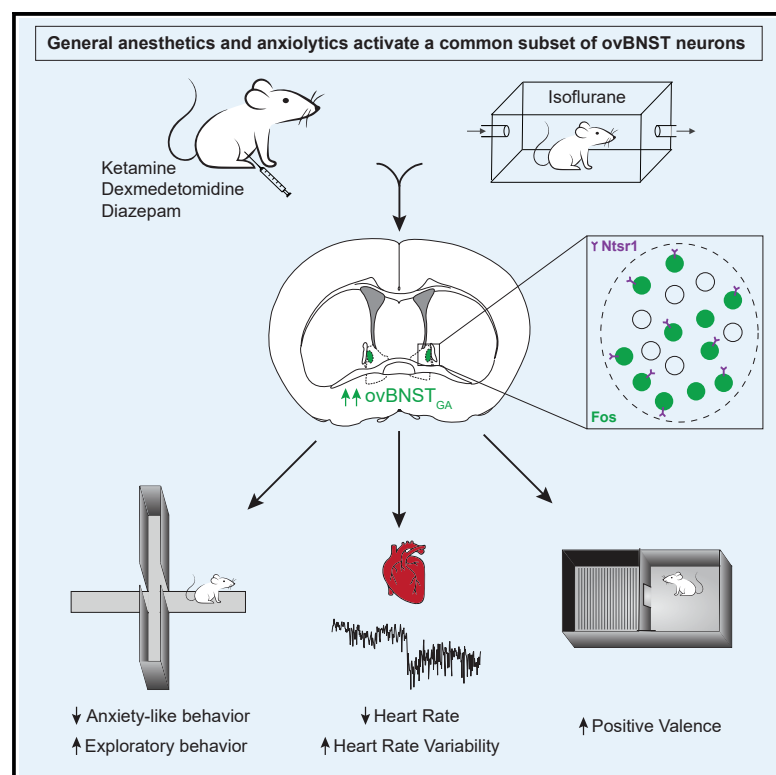# General anesthesia activates a central anxiolytic center in the BNST

Graphical abstract

Authors

Dongye Lu, Camille G. Uldry Lavergne, Seonmi Choi, ..., Bao-Xia Han, Fan Wang, Nitsan Goldstein

Correspondence

fan_wang@mit.edu

In brief

In this paper, Lu et al. characterize a population of neurons in the bed nucleus of the stria terminalis that is activated by general anesthetics and diazepam. These neurons suppress behavioral and autonomic characteristics of anxiety and could be a key mediator of the anxiolytic properties of anesthetics.

Highlights

- General anesthetics and anxiolytics activate a population of neurons in the ovBNST

- Anesthesia-activated ovBNST neurons bidirectionally modulate anxiety-like behavior

- Persistent hyperpolarization of these neurons drives a chronic anxiety-like state

- Activation of these neurons shifts autonomic responses to an anxiolytic state

Article

General anesthesia activates a central anxiolytic center in the BNST

Dongye Lu,[1,2] Camille G. Uldry Lavergne,[1] Seonmi Choi,[1] Jaehong Park,[1,3] Jiwoo Kim,[2] Shengli Zhao,[2] Quinn Desimone,[1] Eva Lendaro,[1] Bin Chen,[1] Bao-Xia Han,[2] Fan Wang,[1,4,*] and Nitsan Goldstein[1]

[1]McGovern Institute for Brain Research, Department of Brain and Cognitive Sciences, Massachusetts Institute of Technology, Cambridge, MA 02139, USA
[2]Department of Neurobiology, Duke University Medical Center, Durham, NC 27710, USA
[3]Department of Biomedical Engineering, Duke University, Durham, NC 27710, USA
[4]Lead contact
*Correspondence: fan_wang@mit.edu
https://doi.org/10.1016/j.celrep.2024.114909

SUMMARY

Low doses of general anesthetics like ketamine and dexmedetomidine have anxiolytic properties independent of their sedative effects, but the underlying mechanisms remain unclear. We discovered a population of GABAergic neurons in the oval division of the bed nucleus of the stria terminalis that are activated by multiple anesthetics and the anxiolytic drug diazepam (ovBNST$_{GA}$). The majority of ovBNST$_{GA}$ neurons express neurotensin receptor 1 (Ntsr1) and form circuits with brain regions known to regulate anxiety and stress responses. Optogenetic activation of ovBNST$_{GA}$ or ovBNST^{Ntsr1} neurons significantly attenuated anxiety-like behaviors in both naive animals and mice with inflammatory pain, while inhibition of these cells elevated anxiety. Activation of these neurons decreased heart rate and increased heart rate variability, suggesting that they reduce anxiety by modulating autonomic responses. Our study identifies ovBNST$_{GA}$/ovBNST^{Ntsr1} neurons as a common neural substrate mediating the anxiolytic effect of low-dose anesthetics and a potential therapeutic target for treating anxiety-related disorders.

INTRODUCTION

Anxiety is characterized as a state of high arousal and negative valence, with an enhanced alertness to threatening cues (or internal imagination and reflection of such cues) that are uncertain or temporally/spatially distant.[1] Anxiety disorders, affecting an estimated 14%–18% of the population at any time, have become one of the most prevalent psychophysiological disorders.[2] Common treatments such as selective serotonin reuptake inhibitors (SSRIs) or benzodiazepines are ineffective in subsets of patients or have abuse potential.[3,4] Thus, there is an urgent need for new and effective treatments for anxiety disorders.

Anesthetics and sedatives used in general anesthesia (GA) have demonstrated anxiolytic properties when used at low doses despite fundamental differences in their mechanisms and biochemical properties.[5–7] For example, in humans, subanesthesia levels of ketamine, an NMDA receptor antagonist, produce robust, quick-onset, and long-lasting anxiolysis on patients with refractory anxiety disorders or social anxiety disorders.[8–10] Dexmedetomidine, an α2-adrenergic receptor agonist, alleviated anxiety-like behaviors in a rodent model of post-traumatic stress disorder (PTSD)[11] and in nerve-ligation-induced chronic pain[12] and has been used to provide peri-operative anxiolysis in animals and human patients.[13–15] Sevoflurane, a GABA receptor potentiator, also reversed the long-term anxiety-like

behaviors caused by a single episode of formalin-induced inflammatory pain in rodents.[16] These observations raise the following question: how do these GA drugs that act on different receptors produce the unified outcome of anxiolysis? Do anesthetics exert their effect by inhibiting anxiogenic circuits or by activating anxiolytic circuits? Is there a common neural target of GA drugs that mediates their anxiolytic effects?

We have previously hypothesized that some of the effects (e.g., sedation and analgesia) of GA are carried out by GA-activated, rather than GA-suppressed, neurons. To this end, we had discovered neurons in the supra optic nucleus that are activated by diverse GA drugs that strongly promote sedation and slow-wave sleep.[17] Similarly, we found a heterogeneous population of GA-activated neurons in the central amygdala (CeA$_{GA}$) that have potent analgesic effects and suppress acute- and chronic-pain-related behaviors.[18] Interestingly, we also identified a cluster of GA-activated neurons located in the oval division of the bed nucleus of the stria terminalis (ovBNST).[18] The ovBNST is a small nucleus within the anterior BNST, which is often considered part of the extended amygdala. In fact, the anterior BNST and CeA share many common inputs and outputs and have largely identical cell type compositions and molecular expression profiles.[19] Importantly, both human and animal studies suggest that the CeA modulates fear responses, while the BNST complex regulates anxiety responses to delayed and/or unpredictable threats.[20,21]
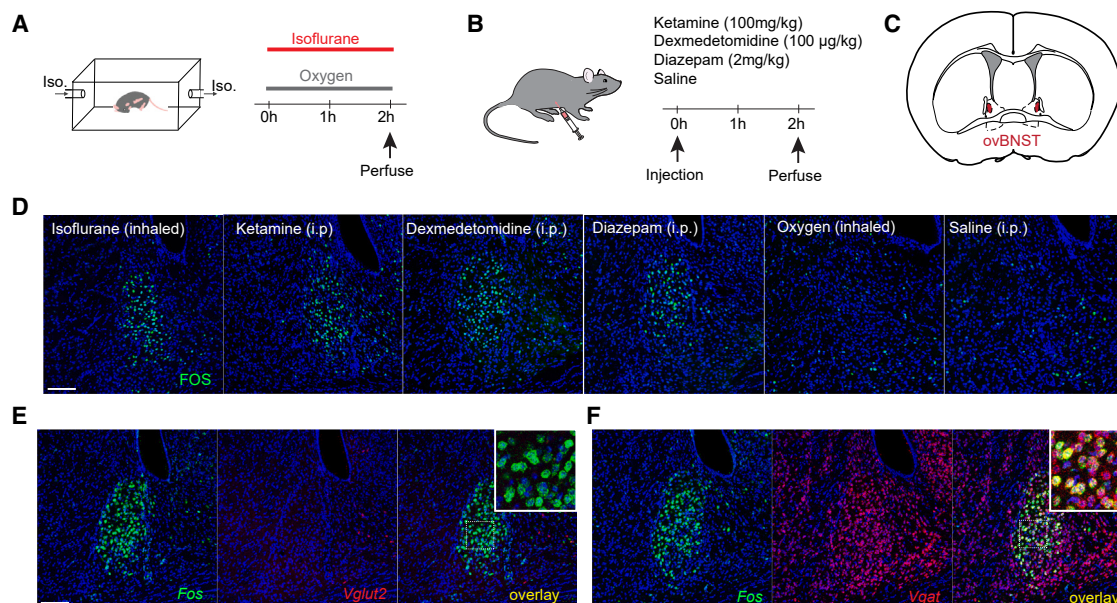
Figure 1. General anesthetics and anxiolytics activate a population of GABAergic neurons in the ovBNST

(A and B) Mice were exposed to inhaled 1.5% isoflurane or control oxygen in a chamber (A) or ketamine, dexmedetomidine, diazepam, or control saline intraperitoneally (B) and sacrificed 2 h later to examine Fos expression.

(C) Depiction of a coronal section of a mouse brain containing the oval nucleus of the BNST (ovBNST).

(D) Representative images showing Fos expression in the ovBNST after each stimulus.

(E) Representative images showing *in situ* hybridization of *Fos* (green) and *Vglut2* (red, to label excitatory neurons). Inset, zoomed-in image of white square in overlay image.

(F) Representative images showing *in situ* hybridization of *Fos* (green) and *Vgat* (red, to label inhibitory neurons). Inset, zoomed-in image of white square in overlay image.

Scale bar, 100 μm.

See also Figure S1.

Given the consensus that the anterior BNST is a critical center for anxiety, we hypothesized that GA-activated ovBNST neurons (hereafter referred to as ovBNST$_{GA}$ neurons) have anxiolytic functions. We characterized the anatomical, molecular, and functional profile of ovBNST$_{GA}$ neurons and found that they are sufficient to drive behavioral and autonomic responses characteristic of an anxiolytic state. Together, our results reveal a specific subpopulation of ovBNST neurons that is a common neural substrate underlying the anxiolytic effects of anesthetic drugs and could be a target for anxiety therapeutics.

RESULTS

Different GA drugs and diazepam all activate a cluster of GABAergic ovBNST neurons

To identify neurons that may underly general-anesthetic-induced anxiolysis, we searched for populations that were activated by both anesthetics and anxiolytic drugs (Figures 1A and 1B). Fos immunostaining revealed a population in the ovBNST (Figure 1C) that was activated by the anesthetics isoflurane, ketamine, and dexmedetomidine, as well as the anxiolytic drug diazepam (a GABA$_A$ receptor agonist; Figure 1D). Saline and oxygen did not induce considerable Fos expression in this region (Figure 1D). Though sexual dimorphism has been observed in BNST circuits, we observed comparable numbers

of isoflurane-activated ovBNST neurons in brains from male and female mice (Figures S1A and S1B). Interestingly, while general anesthetics strongly activate neurons in both the ovBNST and CeA, diazepam's effects were comparatively weaker in the CeA (Figures S1C–S1E; isoflurane activates 153 ± 15 neurons in the CeA vs. 131 ± 3 neurons in the ovBNST per section, $n = 3$, whereas diazepam activates 33 ± 21 neurons in the CeA vs. 82 ± 10 neurons in the ovBNST per section, $n = 3$), suggesting that the ovBNST population (ovBNST$_{GA}$) may be unique in its ability to modulate anxiety.

The BNST consists of many nuclei with both GABAergic and glutamatergic neurons.[22] To determine whether ovBNST$_{GA}$ neurons are predominantly excitatory or inhibitory, we subjected animals to 1 h isoflurane anesthesia and performed *in situ* hybridization for *Fos*, *Vglut2*, or *Vgat* mRNA as markers for glutamatergic or GABAergic cells. We found very sparse *Vglut2* labeling in the ovBNST, and virtually all ovBNST$_{GA}$ neurons were positive for *Vgat* and not *Vglut2*, consistent with results from the Allen Brain Atlas. We therefore concluded that ovBNST$_{GA}$ neurons are GABAergic (Figures 1E and 1F).

Activity-dependent targeting of ovBNST$_{GA}$ neurons

Isoflurane, ketamine, dexmedetomidine, and diazepam have significantly different mechanisms of action, yet all of them activated GABAergic neurons in the ovBNST. Are the same neurons
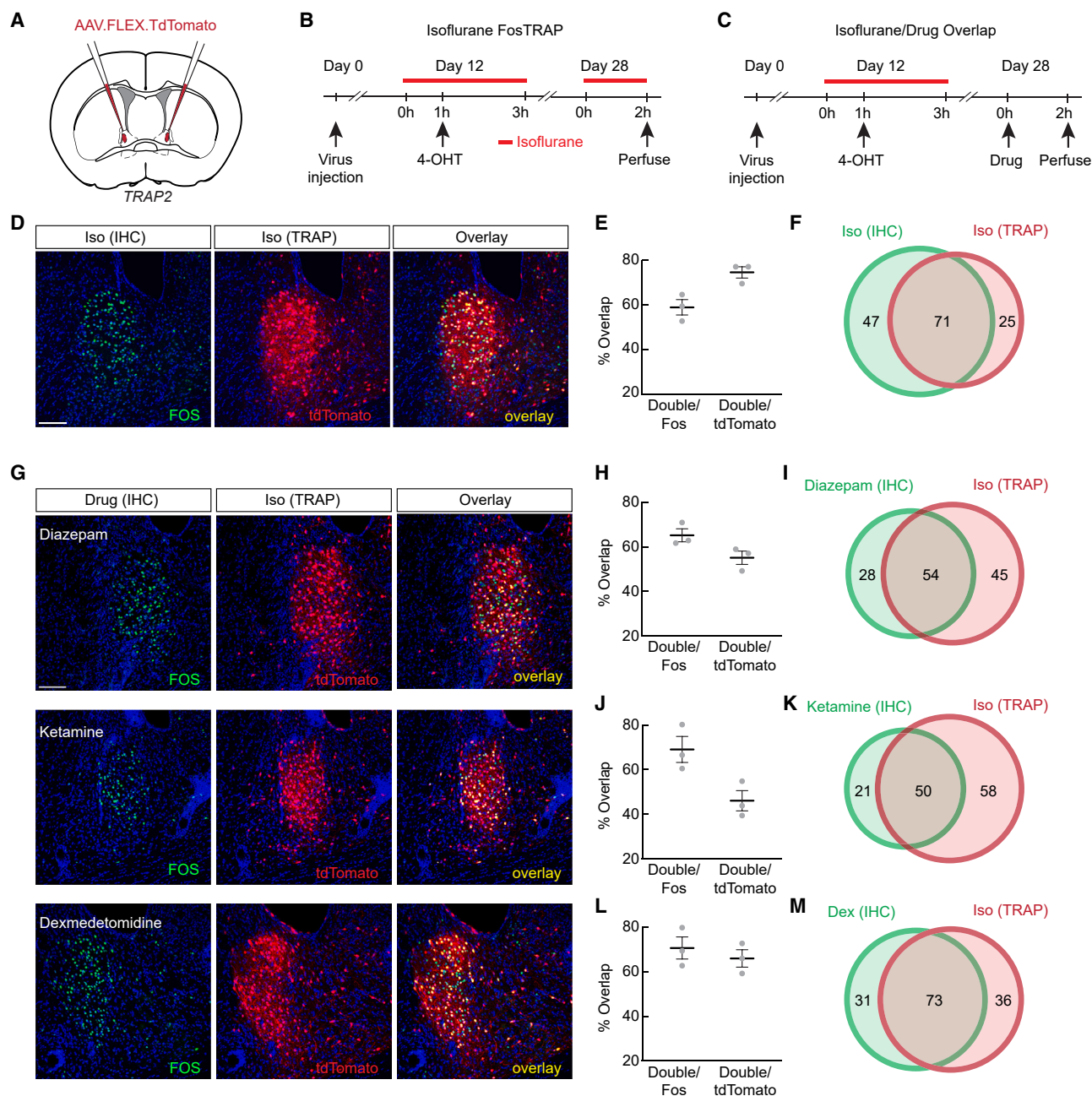
Figure 2. General anesthetics and anxiolytics activate the same subpopulations of ovBNST neurons

(A) Fos-TRAP2 mice were injected with AAV expressing Cre-dependent tdTomato in the ovBNST for activity-dependent labeling.

(B) Experimental timeline for validating activity-dependent labeling of isoflurane-activated neurons (iso-TRAP).

(C) Experimental timeline for examining overlap between cells activated by isoflurane and by other anesthetic and anxiolytic drugs.

(D) Representative images showing Fos immunohistochemistry (IHC; green) and iso-TRAPed neurons (red) after re-exposure to isoflurane.

(E) Percentage of overlap of cells TRAPed by isoflurane exposure and cells expressing Fos after isoflurane re-exposure.

(F) Schematic representation of average overlaps shown in (E).

(G) Representative images showing Fos IHC and iso-TRAPed neurons (red) after exposure to diazepam, ketamine, or dexmedetomidine.

(H) Percentage of overlap of cells TRAPed by isoflurane exposure and cells expressing Fos after i.p. diazepam.

(I) Schematic representation of average overlaps shown in (H).

(J) Percentage of overlap of cells TRAPed by isoflurane exposure and cells expressing Fos after i.p. ketamine.

(K) Schematic representation of average overlaps shown in (J).

activated by these different drugs? We used an activity-dependent method[23] (Targeted Recombination in Active Populations, Fos-TRAP2) to target ovBNST neurons activated by isoflurane (iso-TRAPed neurons), and subsequently re-exposed mice to different general anesthetics and anxiolytic drugs (Figure 2A). Though we have previously used Capturing Activated Neural Ensembles (CANE) to label anesthesia-activated neurons,[17,18] the TRAP method allowed us to use the more diffusible adeno-associated viruses (AAVs) and eliminated the need for precise lentiviral injections into the relatively small ovBNST. First, we confirmed the efficiency and specificity of the labeling by testing whether iso-TRAPed neurons were reactivated by isoflurane (Figure 2B). ∼73% of iso-TRAPed neurons (tdTomato+) were also activated (Fos+) by the second exposure to isoflurane, and ∼57% of Fos+ neurons were tdTomato+ (Figures 2D–2F). Thus, Fos-TRAP2 is a reasonably efficient and selective tool to label and manipulate ovBNST$_{GA}$ neurons.

Next, iso-TRAPed animals were administered ketamine, dexmedetomidine, or diazepam for Fos immunostaining (Figure 2C). We found that all three drugs were able to activate clusters of ovBNST neurons that considerably overlapped with iso-TRAPed cells (Figure 2G). Roughly 55% of iso-TRAPed neurons were activated by diazepam, while ∼65% of the diazepam-activated neurons were iso-TRAPed (Figures 2G–2I). ∼46% of the iso-TRAPed neurons were activated by ketamine, while ∼69% of the ketamine-activated neurons were iso-TRAPed (Figures 2G, 2J, and 2K), and ∼66% of iso-TRAPed neurons were activated by dexmedetomidine, while ∼71% of the dexmedetomidine-activated neurons were iso-TRAPed (Figures 2G, 2L, and 2M). Together, these results highlight the existence of a shared population of ovBNST$_{GA}$ neurons activated by diverse anesthetic/anxiolytic drugs *in vivo*.

To rule out the possibility that the Fos expression we observed was a result of stress induced by anesthesia, we subjected mice to either restraint, foot shocks, or 4% formalin injected bilaterally into the whisker pad and subsequently perfused the animals for Fos immunostaining. None of the stressors led to increased Fos expression in the ovBNST, although the neighboring lateral septum (LS), a region implicated in stress responses,[24–26] showed elevated Fos expression in all three conditions (Figure S2A). We further confirmed the lack of overlap between iso-TRAPed ovBNST$_{GA}$ neurons and the small number of restraint-, foot shock-, or formalin-activated neurons, with restraint activating ∼3.2% of ovBNST$_{GA}$ neurons, foot shock activating ∼4.1% of ovBNST$_{GA}$ neurons, and formalin activating ∼4.6% of ovBNST$_{GA}$ neurons (Figure S2B).

The axonal projection patterns of ovBNST$_{GA}$ neurons
To begin to understand how ovBNST$_{GA}$ neurons integrate into neural circuits involved in modulating anxiety, we examined the axonal projections of ovBNST$_{GA}$ neurons and compared them to previous reports of projection targets from the ovBNST. We in-

jected a Cre-dependent AAV-DIO-GFP virus into the ovBNST and iso-TRAPed these neurons. We found that ovBNST$_{GA}$ neurons densely innervated the anterior-lateral BNST (alBNST) and the ventral BNST (vBNST) (Figure S3B), both of which are known to project extensively to the paraventricular hypothalamus.[27] We found that, consistent with previous reports, ovBNST$_{GA}$ neurons also densely project to the nucleus accumbens (NAc) and the lateral hypothalamus (LH)[28] (Figures S3A and S3D). ovBNST$_{GA}$ neurons sparsely innervate the subthalamic nucleus (STN), the substantia nigra pars compacta or reticulata (SNc/SNr), the periaqueductal gray (PAG), the lateral parabrachial nucleus (lPBN), the reticular formation in hindbrain (Rt), and the medial division of the CeA (CeAm) (Figures S3C–S3H).[29,30] We noted that ovBNST$_{GA}$ cells do not project to CeA$_{GA}$ cells that we previously found to be strongly analgesic (marked by isoflurane-induced Fos expression in the CeA; Figures S3I–S3K).[18] We also observed projections to several areas that have not been previously described, including midline thalamic nuclei (PVT and medial dorsal [MD] nuclei) and the lateral habenula (LHb) (Figure S3D). Of note, many of the axonal targets of ovBNST$_{GA}$ neurons are known to be involved in modulating stress and anxiety-related behaviors.

Activation of ovBNST$_{GA}$ neurons has robust anxiolytic but not analgesic effects
To investigate the functional role of ovBNST$_{GA}$ neurons, we bilaterally injected Cre-dependent AAV vectors into the ovBNST of Fos-TRAP2 mice to express channelrhodopsin-2 (ChR2) for optogenetic activation,[31] enhanced archaerhodopsin (eArch) for optogenetic silencing,[32] or GFP or tdTomato as a control. We then TRAPed ovBNST$_{GA}$ neurons using isoflurane exposure as described above (Figure 3A). We first asked whether these neurons have strong analgesic effects due to their activation by anesthetics as well as our previous findings that GA-activated CeA$_{GA}$ neurons potently suppress pain. We injected formalin unilaterally into the whisker pad and quantified face-wiping behaviors with or without laser stimulation in the ChR2, eArch, or control groups (Figure 3B). Neither activation nor silencing of ovBNST$_{GA}$ neurons had any effect on the amount of time animals spent face wiping, suggesting that ovBNST$_{GA}$ neurons, unlike CeA$_{GA}$ neurons, are not strongly analgesic (Figures 3C–3E).

We next subjected these animals to multiple tests of anxiety-like behavior (open field [OF], elevated plus maze [EPM], and elevated zero maze [EZM]). In rodents, reduced time spent exploring the anxiogenic and open, brightly lit center zone of the OF and open arms of the EPM and EZM are indicative of increased anxiety-like behaviors.[33] We found that 473 nm laser activation in ChR2-ovBNST$_{GA}$ mice significantly increased the time spent exploring the OF center zone (Figures 3F–3I, 3R, and 3S) and the open arms of the EPM (Figures 3J–3M, 3T, and 3U) and EZM (Figures 3N–3Q, 3V, and 3W) compared to the control group. By contrast, 561 nm laser stimulation in the

(L) Percentage of overlap of cells TRAPed by isoflurane exposure and cells expressing Fos after i.p. dexmedetomidine.
(M) Schematic representation of average overlaps shown in (L).

Data are depicted as mean ± SEM. Gray dots represent individual mice. Circle areas in Venn diagrams are proportional to the average numbers of neurons labeled per section. Average number of green only-, red only-, and both red and green-labeled neurons are noted in Venn diagrams. Scale bar, 100 μm.
See also Figures S2 and S3.
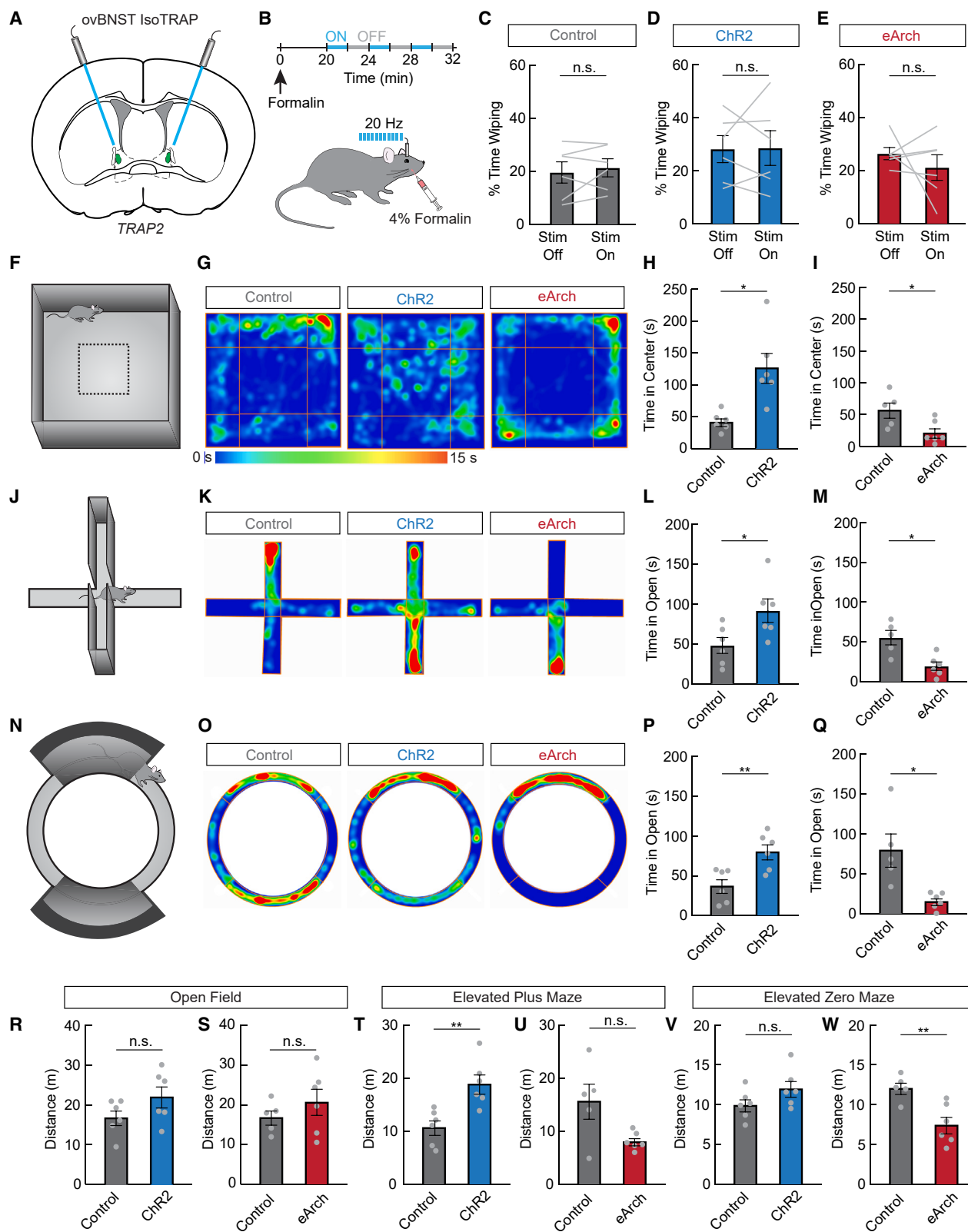
eArch-ovBNST$_{GA}$ mice decreased the time spent exploring these anxiogenic areas in all three behavioral tests compared to controls (Figures 3F–3W). Thus, activation of ovBNST$_{GA}$ neurons is anxiolytic, while inhibition is anxiogenic.

Although we did not observe an effect of acute stimulation of ovBNST$_{GA}$ neurons on pain-elicited self-caring behaviors in the formalin model, anxiety and pain are strongly correlated. Having an anxiety disorder is a strong predictor for the development of chronic pain from an acute injury, and conversely, anxiety is a common symptom of those experiencing chronic pain.[34,35] We thus probed whether ChR2 activation of ovBNST$_{GA}$ neurons could also alleviate anxiety-like behaviors in an inflammatory pain model. We used a bilateral whisker pad injection of complete Freund's adjuvant (CFA).[36,37] Indeed, activation of ovBNST$_{GA}$ neurons in the CFA model resulted in increased exploration to the OF center and EPM and EZM open arms compared to control CFA-injected mice. Thus, ovBNST$_{GA}$ neurons also reduce anxiety-like behaviors during lasting inflammatory pain (Figure S4).

Ntsr1 is a reliable marker for ovBNST$_{GA}$ neurons

Though activity-dependent labeling produced strong behavioral effects when neurons were TRAPed effectively, the success rate of labeling anesthesia-activated ovBNST neurons with this method was low in our hands. We therefore characterized gene expression in ovBNST$_{GA}$ neurons with the goal of finding a molecular marker to target these neurons more efficiently. Given the developmental similarities between the CeA and the anterior BNST,[30] we first examined marker genes known to be expressed in the CeA, including the enzyme *Pkc-delta* (*Pkcd*), the peptides/precursors *Pre-enkephalin* (*Penk1*), *Pre-dynorphin* (*Pdyn*), and *Somatostatin* (*Sst*), and the receptors *Dopamine receptor 1* (*D1r*), *D2r*, and *Neurotensin receptor 1* (*Ntsr1*). Of the

genes tested, the highest overlap with isoflurane-activated neurons occurred with cells positive for *Pkcd*, *Penk1*, and *Ntsr1*. About ~69% of isoflurane-activated *Fos*+ ovBNST neurons expressed *Pkcd*, and ~32% of *Fos*+ neurons expressed *Penk1*. Conversely, ~51% *Pkcd*+ cells and ~30% *Penk1*+ cells were *Fos*+. We also found that ~60% *Fos*+ ovBNST$_{GA}$ neurons express the *Ntsr1* gene encoding the Ntrs1, and ~79% of *Ntsr1*+ cells are *Fos*+ (Figures S5A–S5C). On the other hand, the peptide ligand for Ntsr1, neurotensin (encoded by *Nts*), is expressed by a small population of ovBNST neurons distinct from ovBNST$_{GA}$ cells (Figure S5D). Finally, *in situ* hybridization and immunostaining results showed that ovBNST$_{GA}$ neurons did not overlap with neurons expressing *Pdyn* or *Sst* and had very low levels of expression of dopamine receptors *D1r* and *D2r* (Figure S5D).

Pkcd and *Ntsr1* showed the highest level of overlap with ovBNST$_{GA}$ neurons and were thus good candidates for genetic access to this population. There are three Cre driver lines under the control of either *Pkcd* or *Ntsr1*: BAC-transgenic Pkcd-GluCl-CFP-IRES-Cre (commonly referred to simply as Pkcd-Cre[38]), BAC-transgenic Ntsr1-Cre,[39] and a Ntsr1-Cre knockin line.[40] Since BAC transgenic lines do not fully recapitulate endogenous gene expression patterns, we decided to use the Ntsr1-Cre knockin line to genetically target ovBNST$_{GA}$ neurons. We first injected Cre-dependent AAV-DIO-GFP into the ovBNST of Ntsr1-Cre mice (Ntsr1-GFP) and subsequently subjected these mice to isoflurane anesthesia to induce Fos (Figures 4A and 4B). Overall, ~71% of Fos+ ovBNST$_{GA}$ neurons were labeled by Ntsr1-GFP, while ~52% of the Ntsr1-Cre-GFP+ ovBNST (ovBNST^{Ntsr1}) neurons were Fos+ (Figures 4C and 4D), suggesting that Ntsr1-Cre is a reasonable driver for targeting ovBNST$_{GA}$ neurons.
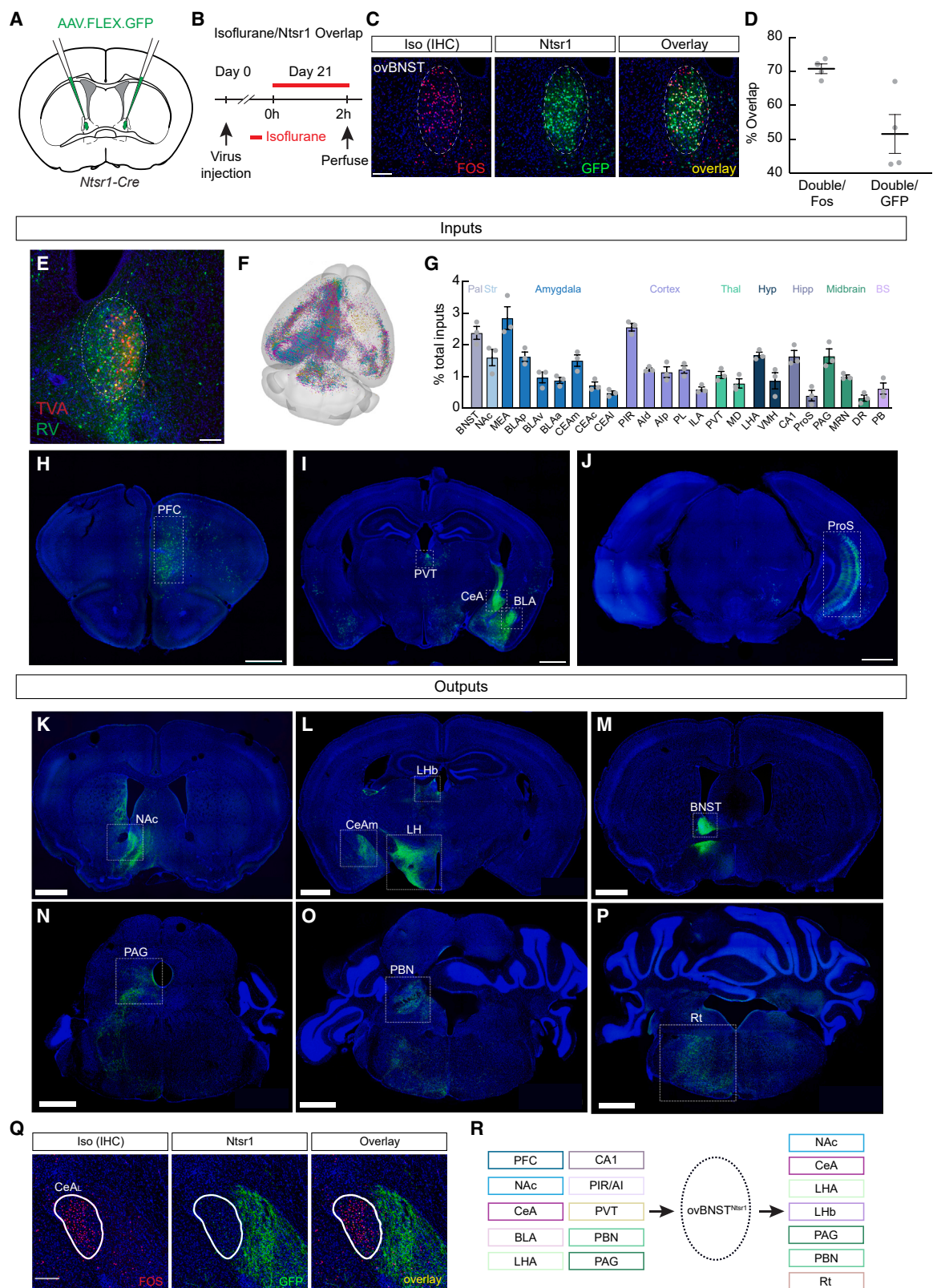
We also used *in vivo* fiber photometry to confirm that ovBNST^{Ntsr1} neurons are activated by general anesthetics. We expressed GCaMP6s in the ovBNST of Ntsr1-Cre mice and

---

Figure 3. ovBNST$_{GA}$ neurons bidirectionally modulate anxiety-like behavior

(A) ovBNST$_{GA}$ neurons were iso-TRAPed to express channelrhodopsin-2 (ChR2), eArchaerhodopsin (eArch), or control GFP bilaterally. Optic fibers were implanted above the injection sites.

(B) Experimental timeline to test the effects of activating or inhibiting ovBNST$_{GA}$ neurons on acute face formalin pain.

(C) Percentage of time spent wiping face during laser-off and laser-on periods in GFP-expressing control mice (n = 6, paired samples t test, n.s.).

(D) Percentage of time spent wiping face during laser-off and laser-on periods in ChR2-expressing mice (n = 6, paired samples t test, n.s.).

(E) Percentage of time spent wiping face during laser-off and laser-on periods in eArch-expressing mice (n = 6, paired samples t test, n.s.).

(F) The open field assay was used to assess general locomotion and anxiety-like behavior.

(G) Representative heatmaps showing a mouse expressing control GFP, ChR2, or eArch during the open field assay. Warmer colors indicate more time spent in that area.

(H) Time spent in the center quarter of the open field in control GFP-expressing mice (gray) or ChR2-expressing mice (blue, n = 6/group, unpaired t test, $p < 0.05$).

(I) Time spent in the center quarter of the open field in control GFP-expressing mice (gray) or eArch-expressing mice (red, n = 5–6/group, unpaired t test, $p < 0.05$).

(J) The elevated plus maze was used to assess anxiety-like behavior.

(K) Representative heatmaps showing a mouse expressing control GFP, ChR2, or eArch during the elevated plus maze assay. Warmer colors indicate more time spent in that area.

(L) Time spent in the open arms of the plus maze in control GFP-expressing mice (gray) or ChR2-expressing mice (blue, n = 6/group, unpaired t test, $p < 0.05$).

(M) Time spent in the open arms of the plus maze in control GFP-expressing mice (gray) or eArch-expressing mice (red, n = 5–6/group, unpaired t test, $p < 0.05$).

(N) The elevated zero maze was used to assess anxiety-like behavior.

(O) Representative heatmaps showing a mouse expressing control GFP, ChR2, or eArch during the elevated zero maze assay. Warmer colors indicate more time spent in that area.

(P) Time spent in the open areas of the zero maze in control GFP-expressing mice (gray) or ChR2-expressing mice (blue, n = 6/group, unpaired t test, $p < 0.01$).

(Q) Time spent in the open areas of the zero maze in control GFP-expressing mice (gray) or eArch-expressing mice (red, n = 5–6/group, unpaired t test, $p < 0.05$).

(R–W) Distance traveled during the open field assay (R, n = 6/group, unpaired t test, n.s.; S, n = 5–6/group, unpaired t test, n.s.), elevated plus maze assay (T, n = 6/group, unpaired t test, $p < 0.01$; U, n = 5–6/group, unpaired t test, n.s.), and elevated zero maze (V, n = 6/group, unpaired t test, n.s.; W, n = 5–6/group, unpaired t test, $p < 0.01$).

Data are depicted as mean ± SEM. Gray dots and lines represent individual mice. t tests: n.s., not significant, *$p < 0.05$, and **$p < 0.01$.

See also Figure S4 and Table S1.

A AAV.FLEX.GFP

Ntsr1-Cre

B Isoflurane/Ntsr1 Overlap

Day 0 — Day 21

Virus injection — Isoflurane — Perfuse

C Iso (IHC) | Ntsr1 | Overlay
ovBNST
FOS | GFP | overlay

D
% Overlap
Double/Fos | Double/GFP

Inputs

E TVA / RV

F

G
Pal Str | Amygdala | Cortex | Thal | Hyp | Hipp | Midbrain | BS
% total inputs
BNST NAc MEA BLAp BLAv BLAa CEAm CEAc CEAl PIR AId AIp PL ILA PVT MD LHA VMH CA1 ProS PAG MRN DR PB

H PFC

I PVT / CeA / BLA

J ProS

Outputs

K NAc

L LHb / CeAm / LH

M BNST

N PAG

O PBN

P Rt

Q Iso (IHC) | Ntsr1 | Overlay
CeA_L
FOS | GFP | overlay

R
PFC | CA1
NAc | PIR/AI
CeA | PVT
BLA | PBN
LHA | PAG
→ ovBNST^Ntsr1 →
NAc
CeA
LHA
LHb
PAG
PBN
Rt

(legend on next page)

implanted an optic fiber to record calcium fluorescence as a proxy for neural activity (Figure S6A). Isoflurane significantly increased GCaMP6s fluorescence (0.8% O2, isoflurane increased from 0% to 2%) compared to oxygen control trials (0% isoflurane, oxygen increased from 0.2% to 0.8%) (Figures S6B–S6D). Taken together, our results demonstrate that Ntsr1 is a reliable marker for most ovBNST$_{GA}$ neurons.

ovBNST^{Ntsr1} neurons are embedded in an extensive limbic network

We next traced both inputs to and outputs of ovBNST^{Ntsr1} neurons. Monosynaptic rabies-mediated presynaptic mapping[41] revealed that ovBNST^{Ntsr1} neurons receive inputs predominantly from the prefrontal cortex (PFC), NAc, CeA, basolateral amygdala (BLA), paraventricular thalamic nucleus (PVT), piriform area, insular cortex, PBN, PAG, and dorsal raphe nucleus (Figures 4E–4J and 4R). Tracing axonal projections from ovBNST^{Ntsr1}-GFP neurons revealed overall similar patterns of projections to those of ovBNST$_{GA}$ neurons, including similar innervation of the CeAm, but not to CeA$_{GA}$ neurons, as well as projections to the NAc, BNST, LHb, PAG, and PBN (compare Figures 4K–4Q to Figure S3). We noted that ovBNST^{Ntsr1} neurons' innervation of many areas, especially in midbrain and hindbrain regions, was denser than that of ovBNST$_{GA}$ neurons, potentially due to the larger number of labeled ovBNST^{Ntsr1} neurons. Overall, the input-output mapping of ovBNST^{Ntsr1} neurons (summarized in Figure 4R) showed that they are embedded in an extensive limbic system neural network.

ovBNST^{Ntsr1} neurons bidirectionally modulate anxiety-like behavior

We next investigated the effect of ovBNST^{Ntsr1} neuron activation on affective and anxiety-like behavior. We expressed ChR2 in ovBNST^{Ntsr1} neurons (Figure 5A) and subjected mice to a conditioned place preference (CPP) assay to test whether activation of these neurons promotes positive affect (Figure 5B). Indeed, mice expressing ChR2, but not control GFP, spent more time in the activation-paired chamber after conditioning,

suggesting that ovBNST^{Ntsr1} neuron activation is inherently pleasant (Figures 5C and 5D). We also found that, like ovBNST$_{GA}$ neuron activation, ChR2 activation of ovBNST^{Ntsr1} neurons led to increased exploration time of the center zone of the OF and the open arms of the EZM (Figures 5E–5L).

With consistent and efficient Ntsr1-Cre-mediated labeling, we asked whether ovBNST^{Ntsr1} neurons might have stronger analgesic effects. We expressed ChR2 in Ntsr1-Cre mice and tested their responses to acute chemical pain (whisker pad formalin), as well as their mechanical and thermal sensitivity before and after CFA-induced inflammatory injury to their paw (Figure 5M). Like activation of iso-TRAPed ovBNST$_{GA}$ neurons, activating ovBNST^{Ntsr1} neurons did not alter self-caring behaviors after a whisker pad formalin injection (Figure 5N). However, we found that ovBNST^{Ntsr1} activation did decrease both mechanical and thermal sensitivity at baseline but was only able to reduce mechanical, but not thermal, sensitivity after CFA injection (Figures 5O and 5P). Together, these results suggest a mild anti-nociceptive effect of ovBNST^{Ntsr1} neurons unlike the much stronger analgesic effects of CeA$_{GA}$ neurons, which are capable of drastically reducing hypersensitivity following both acute pain and chronic neuropathy or inflammation.[18]

Our results show that acutely activating ovBNST^{Ntsr1} neurons reduces anxiety-like behavior and is associated with positive affect. We therefore wondered whether chronically inhibiting these neurons would drive a prolonged anxious state. We expressed the inwardly rectifying potassium channel Kir2.1[42,43] in ovBNST^{Ntsr1} neurons and measured anxiety-like behavior over a 6 week period (Figures 6A and 6B). We also validated the inhibitory effect of Kir2.1 by exposing mice to isoflurane before sacrifice and indeed found reduced Fos expression in the ovBNST in Kir2.1-expressing mice compared to GFP-expressing controls (Figures 6C and 6D). Consistent with previous reports, time spent in the open arms of the EZM was relatively stable in control-GFP mice.[44] In ovBNST^{Ntsr1}-Kir2.1 mice, however, the time spent in the anxiogenic open arms steadily decreased after viral injection over time, indicative of persistent anxiety (Figures 6E and 6F). The total distance traveled was not changed in either

---

Figure 4. Anatomical characterization of ovBNST^{Ntsr1} neurons

(A) GFP was injected into the ovBNST of Ntsr1-Cre mice.

(B) Experimental timeline to confirm isoflurane activation in Ntsr1-Cre-expressing neurons.

(C) Representative images showing Fos+ neurons after isoflurane exposure (red) and GFP-labeled Ntsr1-Cre neurons (green). Scale bar, 100 μm

(D) Percentage of overlap of GFP+ Ntsr1-Cre cells and cells expressing Fos after isoflurane exposure.

(E) Representative image showing Cre-dependent TVA expression (red), rabies expression (green), and both (starter cells, yellow) in the ovBNST. Scale bar, 100 μm.

(F) Rendering of the mouse brain showing the location of all identified inputs. Individual mice are color coded.

(G) Regions with dense inputs to ovBNST^{Ntsr1} neurons. Pal, pallidum; Str; striatum; Thal, thalamus; Hyp, hypothalamus; Hipp, hippocampus; BS, brainstem; BNST, bed nucleus of the stria terminalis; NAc, nucleus accumbens; MEA, medial amygdala; BLAp, BLAv, BLAa, basolateral amygdala posterior, ventral, and anterior parts; CEAm, CEAc, CEAl, central amygdala medial, capsular, and lateral parts; PIR, piriform area; AId, AIp, agranular insular area dorsal and posterior parts; PL, prelimbic area; ILA, infralimbic area; PVT, paraventricular thalamus; MD, mediodorsal thalamus; LHA, lateral hypothalamus; VMH, ventromedial hypothalamus; ProS, prosubiculum; PAG, periaqueductal gray; MRN, midbrain reticular nucleus; DR, dorsal raphe nucleus; PB, parabrachial nucleus.

(H–J) Representative images showing inputs to ovBNST^{Ntsr1} neurons, Scale bar, 1000 μm.

(K–P) Representative images showing ovBNST^{Ntsr1} axonal projections to the NAc (K), the CeAm, lateral habenula (LHb), and LH (L), the BNST (M), the PAG (N), the PBN (O), and the hindbrain reticular nucleus (Rt, P). Scale bar, 1000 μm.

(Q) Representative images showing Fos expression in the lateral CeA (CeA$_L$; left, red) after isoflurane exposure and ovBNST^{Ntsr1} axonal projections to the CeAm showing that ovBNST^{Ntsr1} neurons do not project to CeA$_{GA}$ neurons. Scale bar, 100 μm.

(R) Summary of major inputs to and outputs of ovBNST^{Ntsr1} neurons.

Data are depicted as mean ± SEM. Gray dots represent individual mice.

See also Figure S5.
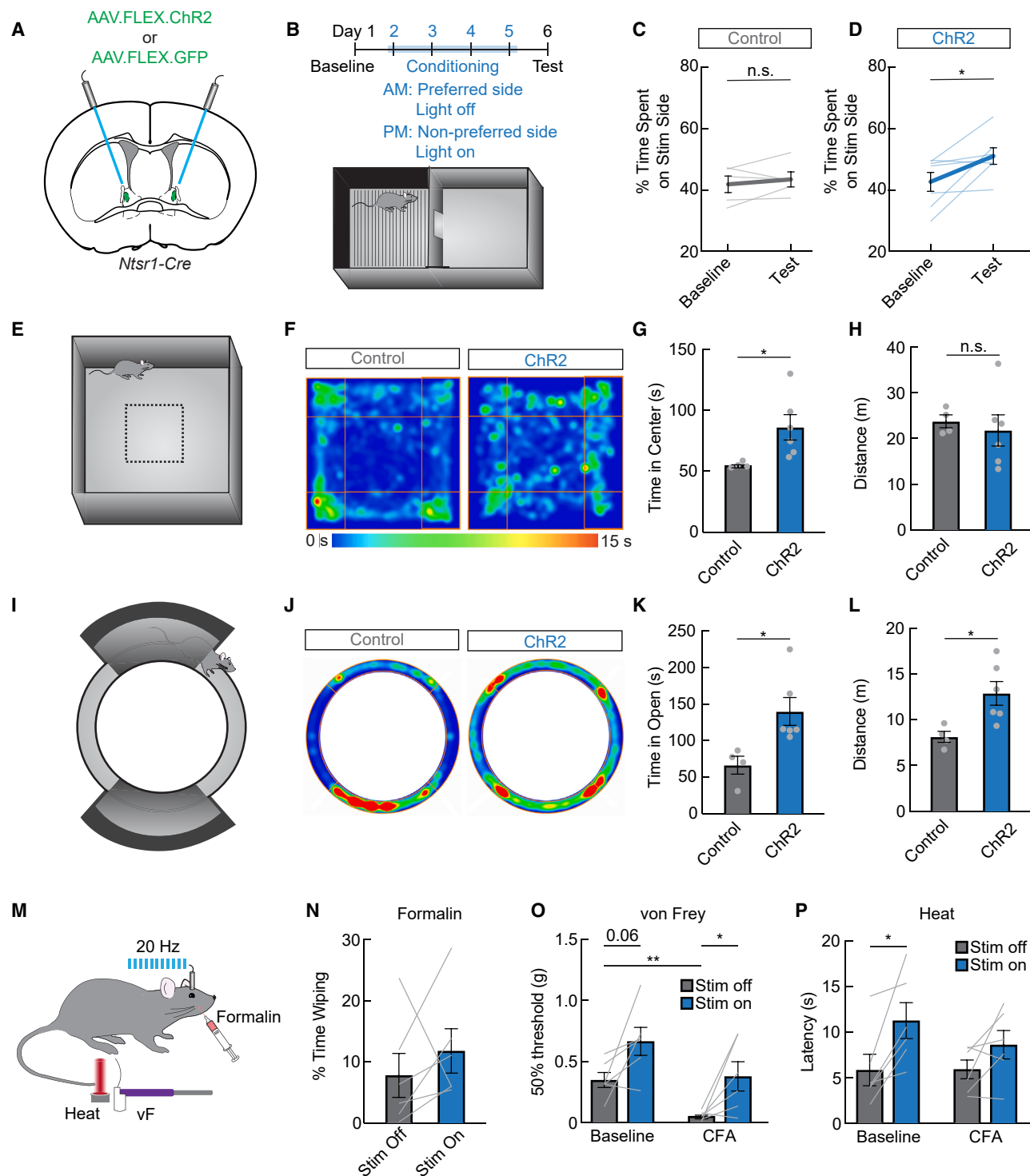
Figure 5. ovBNST^{Ntsr1} neurons are activated by general anesthetics and promote anxiolysis and positive valence

(A) Control GFP or ChR2 was expressed in Ntsr1-Cre mice for optogenetic activation.

(B) Conditioned place preference paradigm. Laser stimulation (stim) was paired with the less preferred side during conditioning.

(C) Percentage of time spent on laser stim side in GFP-expressing control mice ($n = 5$, paired t test, n.s.).

(D) Percentage of time spent on laser stim side in ChR2-expressing mice ($n = 7$, paired t test, $p < 0.05$).

(E) The open field assay was used to assess general locomotion and anxiety-like behavior.

(F) Representative heatmaps showing a mouse expressing control GFP or ChR2 during the open field assay. Warmer colors indicate more time spent in that area.

(legend continued on next page)

group, suggesting that locomotion was not significantly affected (Figure 6G). We also tested mechanical sensitivity using von Frey assays to examine whether a persistently anxious state could cause hypersensitivity. The results showed that the withdrawal threshold was unaffected by the expression of Kir2.1 (Figures 6H–6J). These findings show that optogenetic activation of ovBNST^{Ntsr1} neurons acutely attenuates anxiety-like behavior, while long-term inhibition can induce chronic anxiety-like behavior.

Activation of ovBNST^{Ntsr1} neurons promotes autonomic responses characteristic of an anxiolytic state

While these behavioral studies provided evidence for the anxiolytic function of ovBNST$_{GA}$ and ovBNST^{Ntsr1} activations, the predictive validity of rodent behavioral tests for human anxiety is unclear.[45] In humans, anxiety involves characteristic autonomic nervous system (ANS) responses such as increased heart rate (HR) and shallow breathing. We therefore decided to measure the effect of ovBNST^{Ntsr1} neurons on HR, core body temperature, and breathing.

We implanted telemetric electrocardiogram (ECG) sensors in Ntsr1-Cre mice and expressed either ChR2 or control GFP in ovBNST^{Ntsr1} neurons (Figures 7A–7C). We first tested whether short, continuous activation of ovBNST^{Ntsr1} neurons could affect HR by delivering continuous 473 nm light for 5 s while monitoring ECG signals. Consistent with ovBNST^{Ntsr1} neurons' anxiolytic function, stimulation evoked a significant decrease in HR in ChR2-expressing, but not GFP-expressing, mice (Figures 7D and 7E). We also tested the effects of ovBNST^{Ntsr1} neuron activation over a longer timescale, as mice gradually habituated to the stimulation environment (an unfamiliar empty cage). We stimulated ovBNST^{Ntsr1} neurons at 20 Hz using a 3-min-on, 3-min-off paradigm for 30 min (Figure 7F). We found a significant reduction of HR early in the trial when mice were more anxious (Figure 7G), but the effect of neuronal activation diminished by the final stimulation as animals habituated to the new environment (Figures 7H and 7I), suggesting that the effect of ovBNST^{Ntsr1} is state dependent.

A critical autonomic indicator for anxiogenic vs. anxiolytic state is HR variability (HRV), which reflects the fluctuations of intervals (R-R peak intervals [RRIs]) between successive heart beats. HRV reflects dynamic sympathetic/parasympathetic activity and the body's capacity to quickly shift the balance in preparation for metabolic and homeostatic needs.[46] In anxiety, parasympathetic activity is significantly reduced, whereas sympathetic activity is elevated, resulting in decreased HRV and a more monotonic HR.[47] We analyzed HRV using RMSSD (root mean squared of successive R-R intervals) and compared laser-on vs. -off periods. We found a significant increase in HRV during laser-ON periods in ChR2-ovBNST^{Ntsr1} mice but not GFP-ovBNST^{Ntsr1} controls (Figure 7J). Like the effect on HR, the effect of HRV was stronger in the beginning of the trial (Figures 7J and 7K), while HR decreased and HRV increased in both control and experimental animals gradually as mice habituated to the environment (Figures 7I and 7L). Together, these data suggest that ovBNST^{Ntsr1} neurons could state-dependently regulate autonomic function to suppress anxiety during anxiogenic conditions.

We also used the 5 s continuous laser stimulation protocol to examine ovBNST^{Ntsr1} neurons' effects on respiration. We expected that stimulation would decrease the breathing rate, as slow breathing is associated with calmness, analgesia, anxiolysis, and inhibition of excessive arousal.[48–50] Surprisingly, we observed a significant increase in both the amplitude and frequency of breathing that was reliably and precisely triggered by activation of ovBNST^{Ntsr1} neurons (Figures S7A–S7D). Notably, the simultaneous increases in amplitude and frequency are distinct from the commonly reported shallow breathing, difficulty in inhalation, and tachypnea in anxiety,[51,52] and human studies do report increased breathing rates during certain positive emotions (e.g., excitement, happiness).[53] Thus, it is unclear how the breathing changes we observe correlate with the observed effects of ovBNST^{Ntsr1} neurons on anxiety and affect. Finally, we did not observe any consistent, significant effects of ovBNST^{Ntsr1} neuron stimulation on core body temperature (Figures S7E and S7F).

Overall, our telemetry recordings suggest that ovBNST^{Ntsr1} neurons modulate ANS function by decreasing HR and increasing HRV, thereby shifting the ANS toward a less anxious state. We wondered whether ovBNST^{Ntsr1} neurons are required for the bradycardic effects of anxiolytic drugs. To test this, we tested the effect of diazepam on HR before and after ablation of ovBNST^{Ntsr1}

(G) Time spent in the center quarter of the open field in control GFP-expressing mice (gray) or ChR2-expressing mice (blue, n = 4–6/group, unpaired t test, $p < 0.05$).

(H) Distance traveled during the open field assay in control GFP-expressing mice (gray) or ChR2-expressing mice (blue, n = 4–6/group, unpaired t test, n.s.).

(I) The elevated zero maze was used to assess anxiety-like behavior.

(J) Representative heatmaps showing a mouse expressing control GFP or ChR2 during the elevated zero maze assay. Warmer colors indicate more time spent in that area.

(K) Time spent in the open areas of the elevated zero maze in control GFP-expressing mice (gray) or ChR2-expressing mice (blue, n = 4–6/group, unpaired t test, $p < 0.05$).

(L) Distance traveled during the elevated zero maze assay in control GFP-expressing mice (gray) or ChR2-expressing mice (blue, n = 4–6/group, unpaired t test, $p < 0.05$).
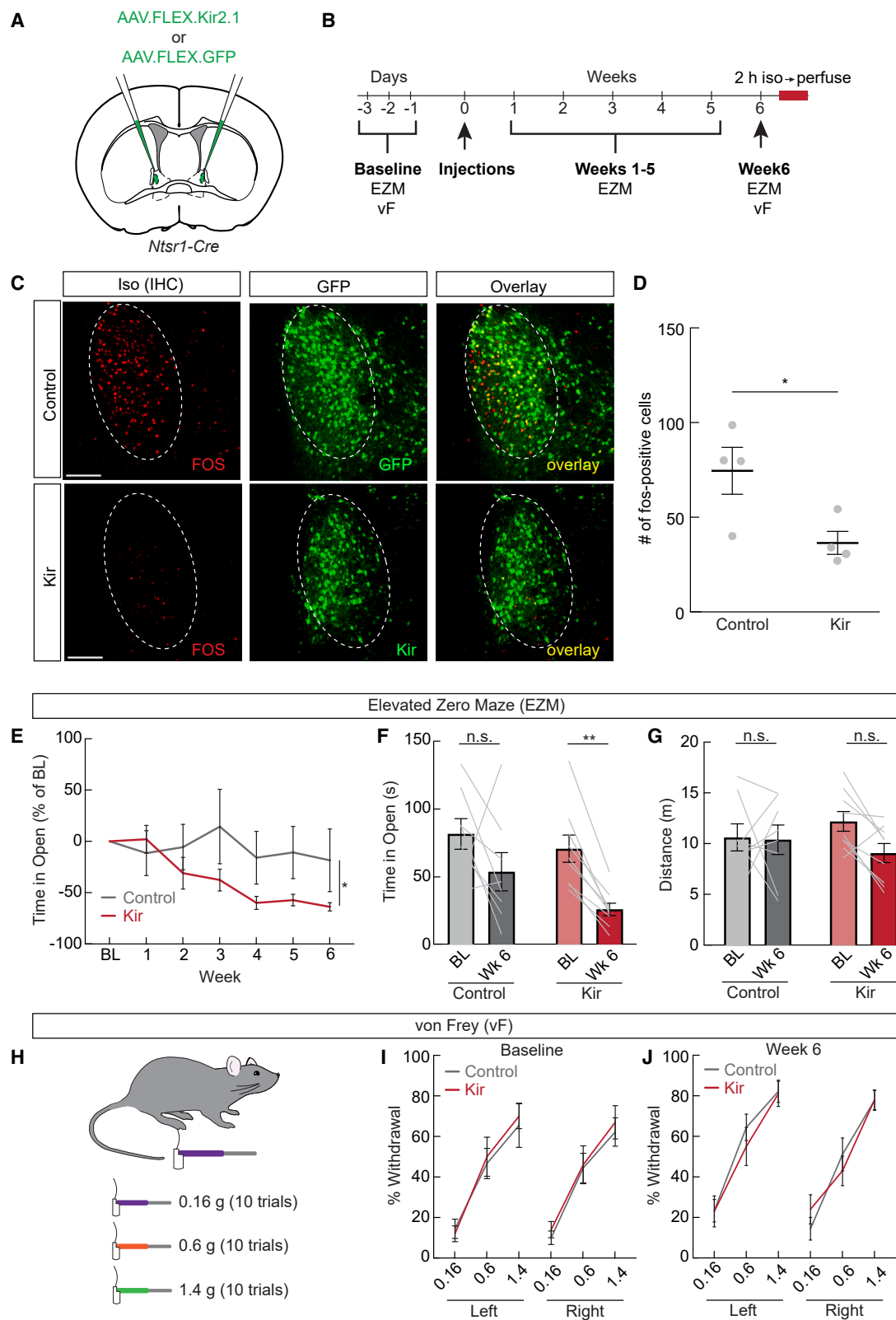
(M) The formalin assay, von Frey test, and Hargreaves heat tests were used to test nociception in ovBNST^{Ntsr1}-ChR2 mice.

(N) Percentage of time spent wiping during stim-off and stim-on bouts after formalin injection in the whisker pad (n = 6, paired t test, n.s.).

(O) Mechanical thresholds with and without stim of ovBNST^{Ntsr1} neurons before and after an injection of CFA in the hindpaw (n = 6, two-way repeated measures ANOVA, main effect of stim $p < 0.05$).

(P) Latency to withdraw from heat with and without stim of ovBNST^{Ntsr1} neurons before and after an injection of CFA in the hindpaw (n = 6, two-way repeated measures ANOVA, main effect of stim $p < 0.05$).

Data are depicted as mean ± SEM. Gray dots and lines represent individual mice. t tests and post hoc comparisons: n.s., not significant, *$p < 0.05$, and **$p < 0.01$. See also Figure S6 and Table S1.

A AAV.FLEX.Kir2.1 or AAV.FLEX.GFP — *Ntsr1-Cre*

B Days / Weeks / 2 h iso→perfuse — Baseline EZM vF / Injections / Weeks 1-5 EZM / Week6 EZM vF

C Iso (IHC) | GFP | Overlay — Control (FOS / GFP / overlay) / Kir (FOS / Kir / overlay)

D # of fos-positive cells — Control vs Kir, *

Elevated Zero Maze (EZM)

E Time in Open (% of BL) vs Week — Control / Kir, *

F Time in Open (s) — BL / Wk 6, Control (n.s.), Kir (**)

G Distance (m) — BL / Wk 6, Control (n.s.), Kir (n.s.)

von Frey (vF)

H 0.16 g (10 trials) / 0.6 g (10 trials) / 1.4 g (10 trials)

I Baseline — % Withdrawal, Control / Kir, Left (0.16, 0.6, 1.4) / Right (0.16, 0.6, 1.4)

J Week 6 — % Withdrawal, Control / Kir, Left (0.16, 0.6, 1.4) / Right (0.16, 0.6, 1.4)

(legend on next page)

neurons (Figure 7M). We expressed the diphtheria toxin receptor (DTR) in ovBNST[Ntsr1] neurons and then implanted mice with telemetric sensors (Figure 7N). Before ablation, diazepam (3 mg/kg, intraperitoneal [i.p.]) significantly reduced the HR compared to a control saline injection (Figure 7O). One week after diphtheria toxin treatment, however, the same dose of diazepam was no longer able to reduce the HR (Figure 7P). These results suggest that ovBNST[Ntsr1] neurons are necessary for the bradycardic effects of the anxiolytic drug diazepam.

DISCUSSION

In this study, we discovered a subpopulation of ovBNST neurons that are commonly activated by diverse general anesthetics and anxiolytics that have different molecular targets. These ovBNST[GA]/ovBNST[Ntsr1] neurons can state-dependently shift both behavioral and ANS responses to a more exploratory, less anxious phenotype. Our data collectively revealed that ovBNST[GA]/ovBNST[Ntsr1] neurons represent a key neural substrate mediating the anxiolytic effect of low-dose general anesthetics and sedatives.

The anterior BNST region has long been known as a major node in the modulation of anxiety. Populations of both anxiogenic and anxiolytic neurons within this region have been described, and it has been suggested that the balance between activity in these populations ultimately determines the overall output of the BNST and its regulation of anxiety.[54,55] Here, we show preferential activation of ovBNST[GA]/ovBNST[Ntsr1] neurons by anxiolytic drugs, but not acute stress, and that this population is strongly anxiolytic. This parallels our previous work that identified a population of anesthesia-activated neurons in the CeA, a region that contains both pro- and anti-nociceptive neural populations.[56] CeA neurons located in the capsular division that receive parabrachial input, for example, are hyperactive following injury and involved in the development of chronic pain.[57] On the contrary, the anesthesia-activated CeA[GA] neurons strongly suppress pain.[18] This raises the possibility that general anesthetics target subpopulations of neurons within GABAergic centers that shift the overall output of these centers to attenuated states of pain or anxiety.

The precise mechanisms through which CeA[GA] and ovBNST[GA] neurons are activated by general anesthetics are

an interesting topic for future investigation. We also show that diazepam preferentially activates ovBNST[GA] neurons compared to CeA[GA] neurons, even though these two sets of cells are known to share embryonic origins and gene expression profiles.[30] Prior studies in acute CeA slices revealed local recurrent inhibitory circuits within the CeA and that diazepam could cause disinhibition of certain populations of CeA neurons,[58] but it is difficult to correlate the concentrations of diazepam used in slice with *in vivo* conditions. Whether the local circuits in the ovBNST further facilitate the disinhibition of ovBNST[GA] neurons by anesthetics and anxiolytics remains to be carefully examined. Future detailed transcriptomic and synaptic connectomic studies of the ovBNST will greatly enable further dissections of this central anxiolytic node and aid in the development of potential treatments for anxiety based on activating ovBNST[GA] neurons. Our finding that ovBNST[GA] neurons express the neurotensin receptor Ntsr1 supports the possibility that endogenous neurotensin signaling in the ovBNST may regulate anxiety. Indeed, small-molecule Ntsr1 agonists have been pursued for decades as potential therapeutics for treating conditions such as pain, schizophrenia, obesity, and addiction.[59–61] While we do not know the precise role or source of neurotensin signaling in the GA-mediated activation of ovBNST[Ntsr1] neurons, we noted that ovBNST neurotensin-expressing (Nts+) neurons are not activated by anesthetics (Figure S5D). Thus, local release is not required for anesthetics to activate ovBNST[Ntsr1] neurons. Our study should further fuel interest in developing Ntsr1 agonists as treatments for diverse neurologic and psychiatric diseases.

Autonomic responses are an integral component of all emotions, including anxiety. The relative ease of collecting autonomic measurements in humans has resulted in a plethora of data on the relationship between physiological responses and various emotional and disease states. For example, generalized anxiety disorder and a number of chronic pain conditions are consistently associated with reduced HRV.[47,62,63] Yet, most animal studies rely solely on motor behaviors without measuring autonomic output. Mice are prey animals and are known to hide their behavioral responses to pain and stress; thus, measuring these behaviors alone may be insufficient to determine their affective/emotional state. For example, while the

---

Figure 6. Chronic inactivation of ovBNST[Ntsr1] neurons drives long term anxiety-like behavior

(A) Control AAV-DiO-GFP or AAV-DiO-Kir2.1 was expressed in Ntsr1-Cre mice for chronic inhibition.

(B) Experimental timeline for chronic inhibition experiments. Elevated zero maze (EZM) and von Frey (vF) tests were performed before and after viral injections in both control and experimental mice.

(C) Representative images showing isoflurane-induced Fos (red) and viral expression (green) in control GFP and Kir2.1 mice. Scale bar, 100 μm.

(D) Number of Fos+ neurons per section in the ovBNST of control GFP- and Kir2.1-expressing mice after isoflurane exposure ($n = 4$/group, unpaired t test, $p < 0.05$).

(E) Time spent in the open arms of the EZM (percentage of baseline [BL]) in control (gray) and Kir2.1-expressing (red) mice ($n = 8$–9/group, two-way repeated measures ANOVA, $p < 0.05$).

(F) Time spent in the open arms of the EZM during the BL and week 6 tests ($n = 8$–9/group, two-way repeated measures ANOVA, Kir2.1 BL vs. week 6 $p < 0.01$).

(G) Total distance traveled during the EZM assay during the BL and week 6 tests ($n = 8$–9/group, two-way repeated measures ANOVA, n.s.).

(H) The vF test was used to determine whether chronic inhibition of ovBNST[Ntsr1] neurons affects mechanical sensitivity.

(I) Percentage of withdrawal during the vF test before viral injections ($n = 8$–9/group, two-way repeated measures ANOVA, n.s.).

(J) Percentage of withdrawal during the vF test 6 weeks after viral injections ($n = 8$–9/group, two-way repeated measures ANOVA, n.s.).

Data are depicted as mean ± SEM. Gray dots and lines represent individual mice. t tests, interactions, and post hoc comparisons: n.s., not significant, *$p < 0.05$, and **$p < 0.01$.

See also Table S1.
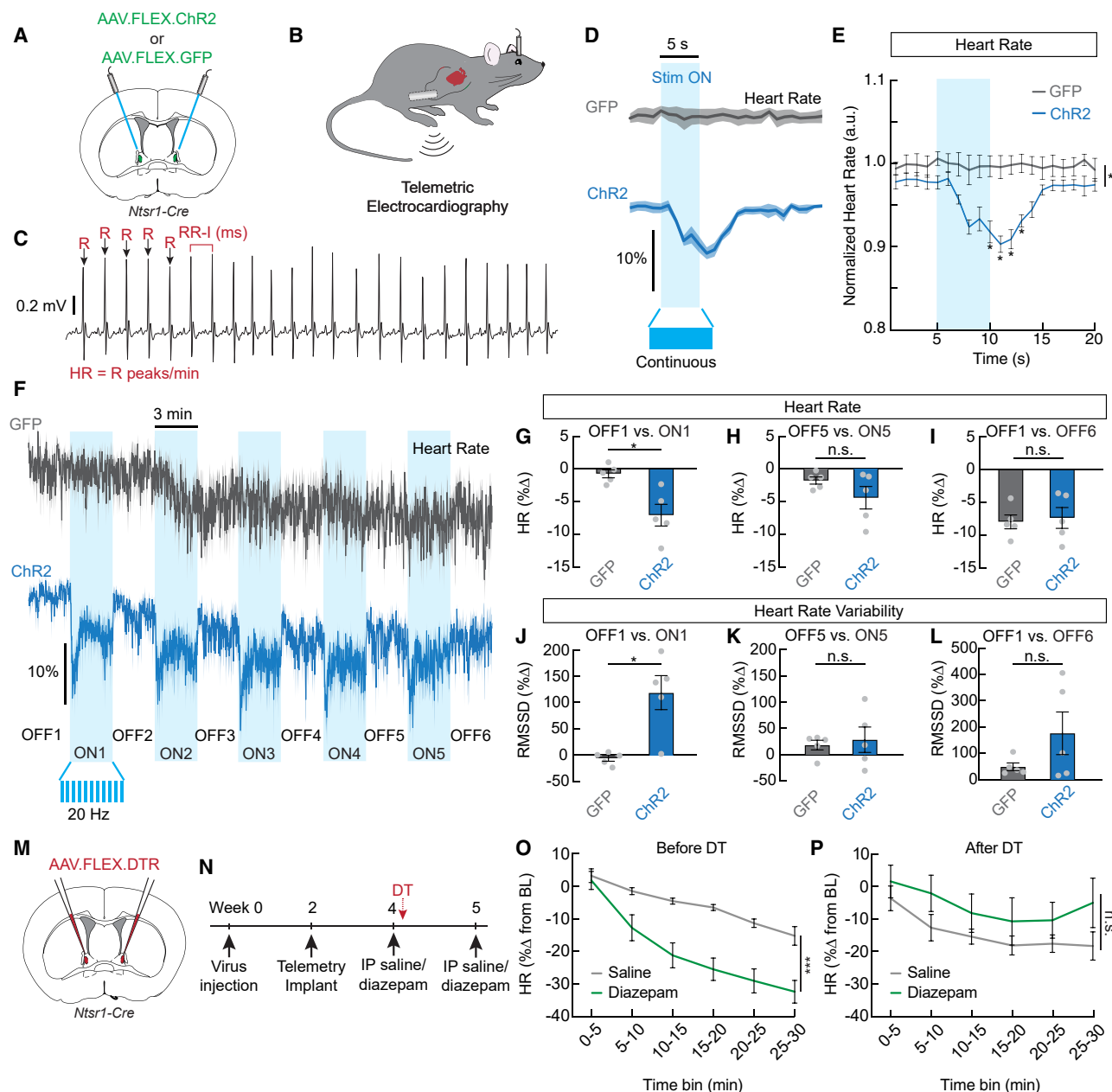
Figure 7. ovBNST^Ntsr1 neurons shift autonomic output to a less anxious state

(A) Control GFP or ChR2 was expressed in Ntsr1-Cre mice for optogenetic activation.

(B) Wireless telemetry sensors were implanted in the abdomen, with electrodes implanted in the chest.

(C) Example raw electrocardiography (ECG) trace showing R peaks (arrows). Heart rate was calculated as R peaks/min, and heart rate variability was calculated from RR intervals or the time between successive R peaks.

(D) Average normalized heart rate in GFP-expressing mice (gray) and ChR2-expressing mice (blue) during a 5 s continuous stimulation (stim) with 473 nm laser. Dark lines represent mean, and lighter shaded areas represent SEM.

(E) Mean normalized heart rate from the recordings shown in (D) ($n = 5$/group, two-way repeated measures ANOVA, $p < 0.001$).

(F) Average normalized heart rate in GFP-expressing mice (gray) and ChR2-expressing mice (blue) during a 33 min trial where 20 Hz 473 nm light was delivered in a 3-min-off, 3-min-on paradigm.

(G) Change in heart rate during the first stim-on period compared to the first stim-off period in GFP- and ChR2-expressing mice ($n = 5$/group, unpaired t test, $p < 0.05$).

(H) Change in heart rate during the fifth stim-on period compared to the fifth stim-off period in GFP- and ChR2-expressing mice ($n = 5$/group, unpaired t test, n.s.).

(I) Change in heart rate during the sixth stim-off period compared to the first stim-off period in GFP- and ChR2-expressing mice ($n = 5$/group, unpaired t test, n.s.).

(legend continued on next page)

opposing anxiolytic and anxiogenic effects of *Pkcd*+ BNST neurons from different studies[58,64,65] may be caused by heterogeneity in the *Pkcd*+ population, it is possible that the ambiguity of behavioral readouts in different experimental environments is a factor as well. We argue that adding an autonomic response measurement such as HR and HRV will go a long way to improve the validity of pre-clinical animal studies aimed at identifying circuit and molecular targets for treating anxiety and other emotional or affective disorders. Here, we show that activating ovBNST[Ntsr1] neurons reduces HR and increases HRV, whereas ablating these neurons abolished the bradycardic effect of the anxiolytic drug diazepam. These findings support the idea that ovBNST[Ntsr1] neurons reduce anxiety in part through controlling ANS responses. The links between GA-activated neurons and ANS function may also explain why low doses of general anesthetics have anxiolytic and analgesic properties. At high doses, shifting the sympathetic/parasympathetic balance to a parasympathetically dominant state causes sedation. At lower doses, the mild reduction in sympathetic tone is sufficient for anxiolysis and analgesia through activation of a GA-activated inhibitory network that does not affect overall arousal.

In conclusion, we have identified a population of neurons in the ovBNST that are activated by general anesthetics and anxiolytic drugs. Most of these neurons express *Ntsr1* and project to limbic areas involved in motivation, affect, and autonomic control. Activating these neurons suppresses both behavioral and autonomic hallmarks of anxiety. These findings suggest that ovBNST[Ntsr1] neurons are a crucial node for the anxiolytic effects of low-dose general anesthetics.

Limitations of the study

We note several limitations in our study that future work could address. First, while we found that ovBNST[Ntsr1] neurons are important for the bradycardic effects of diazepam, our study did not test the behavioral effects of low doses of general anesthetics or anxiolytics and whether ovBNST[GA]/ovBNST[Ntsr1] neurons are required for these effects. We also did not test the ability of ovBNST[GA]/ovBNST[Ntsr1] neurons to suppress anxiety in chronically stressed animals, which may better model human anxiety. Finally, due to the challenges of consistently labeling ovBNST[GA] neurons using Fos-TRAP, we only tested reflexive pain responses in ovBNST[Ntsr1] neurons but not ovBNST[GA] neurons.

STAR★METHODS

Detailed methods are provided in the online version of this paper and include the following:

- KEY RESOURCES TABLE
- EXPERIMENTAL MODEL AND STUDY PARTICIPANT DETAILS
- METHOD DETAILS
  - Histology
  - Drugs
  - IsoTRAP
  - Surgery
  - Optogenetic activation and inhibition
  - Fiber photometry
  - Behavioral assays
  - Complete Freund's adjuvant (CFA)-induced persistent inflammation

(J) Change in heart rate variability (RMSSD, root mean squared of successive RR intervals) during the first stim-on period compared to the first stim-off period in GFP- and ChR2-expressing mice ($n = 5$/group, unpaired t test, $p < 0.05$).

(K) Change in heart rate variability (RMSSD) during the fifth stim-on period compared to the fifth stim-off period in GFP and ChR2-expressing mice ($n = 5$/group, unpaired t test, n.s.).

(L) Change in heart rate variability (RMSSD) during the sixth stim-off period compared to the first stim-off period in GFP- and ChR2-expressing mice ($n = 5$/group, unpaired t test, n.s.).

(M) Diphtheria toxin receptor (DTR) was expressed in Ntsr1-Cre mice for conditional ablation of ovBNST[Ntsr1] neurons.

(N) Timeline depicting ablation experiment to determine the necessity of ovBNST[Ntsr1] neurons for the bradycardic effects of diazepam.

(O) Change in heart rate from a 10 min baseline following intraperitoneal injection of saline or diazepam before ablation (3 mg/kg, $n = 4$, two-way repeated measures ANOVA, main effect of drug $p < 0.001$).

(P) Change in heart rate from a 10 min baseline following intraperitoneal injection of saline or diazepam after ablation (3 mg/kg, $n = 4$, two-way repeated measures ANOVA, main effect of drug n.s.).

Data are depicted as mean ± SEM. Gray dots and lines represent individual mice. t tests, ANOVA main effects, and post hoc comparisons: n.s., not significant; $^*p < 0.05$, $^{**}p < 0.01$, and $^{***}p < 0.001$.

See also Figure S7 and Table S1.

○ Telemetry and breathing
● QUANTIFICATION AND STATISTICAL ANALYSIS

REFERENCES

1. Calhoon, G.G., and Tye, K.M. (2015). Resolving the neural circuits of anxiety. Nat. Neurosci. *18*, 1394–1404. https://doi.org/10.1038/nn.4101.

2. Ströhle, A., Gensichen, J., and Domschke, K. (2018). The Diagnosis and Treatment of Anxiety Disorders. Dtsch. Arztebl. Int. *155*, 611–620. https://doi.org/10.3238/arztebl.2018.0611.

3. Bachhuber, M.A., Hennessy, S., Cunningham, C.O., and Starrels, J.L. (2016). Increasing Benzodiazepine Prescriptions and Overdose Mortality in the United States, 1996-2013. Am. J. Publ. Health *106*, 686–688. https://doi.org/10.2105/ajph.2016.303061.

4. Lader, M.H. (1999). Limitations on the use of benzodiazepines in anxiety and insomnia: are they justified? Eur. Neuropsychopharmacol *9*, S399–S405. https://doi.org/10.1016/s0924-977x(99)00051-6.

5. Brechmann, T., Maier, C., Kaisler, M., Vollert, J., Schmiegel, W., Pak, S., Scherbaum, N., Rist, F., and Riphaus, A. (2018). Propofol sedation during gastrointestinal endoscopy arouses euphoria in a large subset of patients. United European Gastroenterol. J. *6*, 536–546. https://doi.org/10.1177/2050640617736231.

6. Gaffney, B.J. (2007). Anesthesia, analgesia, and euphoria. Biophys. J. *92*, 1–2. https://doi.org/10.1529/biophysj.106.096503.

7. Zeidan, A., and Baraka, A. (2004). Is euphoria a side-effect of lidocaine? Anaesthesia *59*, 1253–1254. https://doi.org/10.1111/j.1365-2044.2004.04025.x.

8. Glue, P., Medlicott, N.J., Harland, S., Neehoff, S., Anderson-Fahey, B., Le Nedelec, M., Gray, A., and McNaughton, N. (2017). Ketamine's dose-related effects on anxiety symptoms in patients with treatment refractory anxiety disorders. J. Psychopharmacol. *31*, 1302–1305. https://doi.org/10.1177/0269881117705089.

9. Irwin, S.A., Iglewicz, A., Nelesen, R.A., Lo, J.Y., Carr, C.H., Romero, S.D., and Lloyd, L.S. (2013). Daily oral ketamine for the treatment of depression and anxiety in patients receiving hospice care: a 28-day open-label proof-of-concept trial. J. Palliat. Med. *16*, 958–965. https://doi.org/10.1089/jpm.2012.0617.

10. Taylor, J.H., Landeros-Weisenberger, A., Coughlin, C., Mulqueen, J., Johnson, J.A., Gabriel, D., Reed, M.O., Jakubovski, E., and Bloch, M.H. (2018). Ketamine for Social Anxiety Disorder: A Randomized, Placebo-Controlled Crossover Trial. Neuropsychopharmacology *43*, 325–333. https://doi.org/10.1038/npp.2017.194.

11. Ji, M.H., Jia, M., Zhang, M.Q., Liu, W.X., Xie, Z.C., Wang, Z.Y., and Yang, J.J. (2014). Dexmedetomidine alleviates anxiety-like behaviors and cognitive impairments in a rat model of post-traumatic stress disorder. Prog. Neuro-Psychopharmacol. Biol. Psychiatry *54*, 284–288. https://doi.org/10.1016/j.pnpbp.2014.06.013.

12. Gao, W., Long, D.-d., Pan, T.-t., Hu, R., Chen, D.-y., Mao, Y., Chai, X.-q., Jin, Y., Zhang, Z., and Wang, D. (2022). Dexmedetomidine alleviates anxiety-like behavior in mice following peripheral nerve injury by reducing the hyperactivity of glutamatergic neurons in the anterior cingulate cortex. Biochem. Pharmacol. *206*, 115293. https://doi.org/10.1016/j.bcp.2022.115293.

13. Boyer, J. (2009). Treating agitation with dexmedetomidine in the ICU. Dimens. Crit. Care Nurs. *28*, 102–109. https://doi.org/10.1097/DCC.0b013e31819aef3d.

14. Korpivaara, M., Huhtinen, M., Aspegrén, J., and Overall, K. (2021). Dexmedetomidine oromucosal gel reduces fear and anxiety in dogs during veterinary visits: A randomised, double-blind, placebo-controlled clinical pilot study. Vet. Rec. *189*, e832. https://doi.org/10.1002/vetr.832.

15. Zeng, W., Chen, L., Liu, X., Deng, X., Huang, K., Zhong, M., Zhou, S., Zhan, L., Jiang, Y., and Liang, W. (2022). Intranasal Dexmedetomidine for the Treatment of Pre-operative Anxiety and Insomnia: A Prospective, Randomized, Controlled, and Clinical Trial. Front. Psychiatr. *13*, 816893. https://doi.org/10.3389/fpsyt.2022.816893.

16. Luo, C., Zhang, Y.-L., Luo, W., Zhou, F.H., Li, C.-Q., Xu, J.-M., and Dai, R.-P. (2015). Differential effects of general anesthetics on anxiety-like behavior in formalin-induced pain: involvement of ERK activation in the anterior cingulate cortex. Psychopharmacology *232*, 4433–4444. https://doi.org/10.1007/s00213-015-4071-2.

17. Jiang-Xie, L.F., Yin, L., Zhao, S., Prevosto, V., Han, B.X., Dzirasa, K., and Wang, F. (2019). A Common Neuroendocrine Substrate for Diverse General Anesthetics and Sleep. Neuron *102*, 1053–1065.e4. https://doi.org/10.1016/j.neuron.2019.03.033.

18. Hua, T., Chen, B., Lu, D., Sakurai, K., Zhao, S., Han, B.-X., Kim, J., Yin, L., Chen, Y., Lu, J., and Wang, F. (2020). General anesthetics activate a potent central pain-suppression circuit in the amygdala. Nat. Neurosci. *23*, 854–868. https://doi.org/10.1038/s41593-020-0632-8.

19. Walker, D.L., and Davis, M. (2008). Role of the extended amygdala in short-duration versus sustained fear: a tribute to Dr. Lennart Heimer. Brain Struct. Funct. *213*, 29–42. https://doi.org/10.1007/s00429-008-0183-3.

20. Avery, S.N., Clauss, J.A., and Blackford, J.U. (2016). The Human BNST: Functional Role in Anxiety and Addiction. Neuropsychopharmacology *41*, 126–141. https://doi.org/10.1038/npp.2015.185.

21. Lebow, M.A., and Chen, A. (2016). Overshadowed by the amygdala: the bed nucleus of the stria terminalis emerges as key to psychiatric disorders. Mol. Psychiatr. *21*, 450–463. https://doi.org/10.1038/mp.2016.1.

22. Stamatakis, A.M., Sparta, D.R., Jennings, J.H., McElligott, Z.A., Decot, H., and Stuber, G.D. (2014). Amygdala and bed nucleus of the stria terminalis circuitry: Implications for addiction-related behaviors. Neuropharmacology *76*, 320–328. https://doi.org/10.1016/j.neuropharm.2013.05.046.

23. DeNardo, L.A., Liu, C.D., Allen, W.E., Adams, E.L., Friedmann, D., Fu, L., Guenthner, C.J., Tessier-Lavigne, M., and Luo, L. (2019). Temporal evolution of cortical ensembles promoting remote memory retrieval. Nat. Neurosci. *22*, 460–469. https://doi.org/10.1038/s41593-018-0318-7.

24. Anthony, T.E., Dee, N., Bernard, A., Lerchner, W., Heintz, N., and Anderson, D.J. (2014). Control of Stress-Induced Persistent Anxiety by an Extra-Amygdala Septohypothalamic Circuit. Cell *156*, 522–536. https://doi.org/10.1016/j.cell.2013.12.040.

25. Wang, D., Pan, X., Zhou, Y., Wu, Z., Ren, K., Liu, H., Huang, C., Yu, Y., He, T., Zhang, X., et al. (2023). Lateral septum-lateral hypothalamus circuit dysfunction in comorbid pain and anxiety. Mol. Psychiatr. *28*, 1090–1100. https://doi.org/10.1038/s41380-022-01922-y.

26. Xu, Y., Lu, Y., Cassidy, R.M., Mangieri, L.R., Zhu, C., Huang, X., Jiang, Z., Justice, N.J., Xu, Y., Arenkiel, B.R., and Tong, Q. (2019). Identification of a neurocircuit underlying regulation of feeding by stress-related emotional responses. Nat. Commun. *10*, 3446. https://doi.org/10.1038/s41467-019-11399-z.

27. Gungor, N.Z., and Paré, D. (2016). Functional Heterogeneity in the Bed Nucleus of the Stria Terminalis. J. Neurosci. *36*, 8038. https://doi.org/10.1523/JNEUROSCI.0856-16.2016.

28. Giardino, W.J., Eban-Rothschild, A., Christoffel, D.J., Li, S.-B., Malenka, R.C., and de Lecea, L. (2018). Parallel circuits from the bed nuclei of stria terminalis to the lateral hypothalamus drive opposing emotional states. Nat. Neurosci. *21*, 1084–1095. https://doi.org/10.1038/s41593-018-0198-x.

29. Dong, H.-W., Petrovich, G.D., Watts, A.G., and Swanson, L.W. (2001). Basic organization of projections from the oval and fusiform nuclei of the bed nuclei of the stria terminalis in adult rat brain. J. Comp. Neurol. *436*, 430–455. https://doi.org/10.1002/cne.1079.

30. Ye, J., and Veinante, P. (2019). Cell-type specific parallel circuits in the bed nucleus of the stria terminalis and the central nucleus of the amygdala of the mouse. Brain Struct. Funct. *224*, 1067–1095. https://doi.org/10.1007/s00429-018-01825-1.

31. Boyden, E.S., Zhang, F., Bamberg, E., Nagel, G., and Deisseroth, K. (2005). Millisecond-timescale, genetically targeted optical control of neural activity. Nat. Neurosci. *8*, 1263–1268. https://doi.org/10.1038/nn1525.

32. Mattis, J., Tye, K.M., Ferenczi, E.A., Ramakrishnan, C., O'Shea, D.J., Prakash, R., Gunaydin, L.A., Hyun, M., Fenno, L.E., Gradinaru, V., et al. (2011). Principles for applying optogenetic tools derived from direct comparative analysis of microbial opsins. Nat. Methods *9*, 159–172. https://doi.org/10.1038/nmeth.1808.

33. Lezak, K.R., Missig, G., and Carlezon Jr, W.A. (2017). Behavioral methods to study anxiety in rodents. Dialogues Clin. Neurosci. *19*, 181–191. https://doi.org/10.31887/DCNS.2017.19.2/wcarlezon.

34. Bushnell, M.C., Ceko, M., and Low, L.A. (2013). Cognitive and emotional control of pain and its disruption in chronic pain. Nat. Rev. Neurosci. *14*, 502–511. https://doi.org/10.1038/nrn3516.

35. Villemure, C., and Bushnell, M.C. (2009). Mood influences supraspinal pain processing separately from attention. J. Neurosci. *29*, 705–715. https://doi.org/10.1523/jneurosci.3822-08.2009.

36. Parent, A.J., Beaudet, N., Beaudry, H., Bergeron, J., Bérubé, P., Drolet, G., Sarret, P., and Gendron, L. (2012). Increased anxiety-like behaviors in rats experiencing chronic inflammatory pain. Behav. Brain Res. *229*, 160–167. https://doi.org/10.1016/j.bbr.2012.01.001.

37. Spinieli, R.L., Cazuza, R.A., Sales, A.J., Carolino, R.O.G., Martinez, D., Anselmo-Franci, J., Tajerian, M., and Leite-Panissi, C.R. (2022). Persistent inflammatory pain is linked with anxiety-like behaviors, increased blood corticosterone, and reduced global DNA methylation in the rat amygdala. Mol. Pain *18*, 17448069221121307. https://doi.org/10.1177/17448069221121307.

38. Haubensak, W., Kunwar, P.S., Cai, H., Ciocchi, S., Wall, N.R., Ponnusamy, R., Biag, J., Dong, H.W., Deisseroth, K., Callaway, E.M., et al. (2010). Genetic dissection of an amygdala microcircuit that gates conditioned fear. Nature *468*, 270–276. https://doi.org/10.1038/nature09553.

39. Gong, S., Doughty, M., Harbaugh, C.R., Cummins, A., Hatten, M.E., Heintz, N., and Gerfen, C.R. (2007). Targeting Cre recombinase to specific neuron populations with bacterial artificial chromosome constructs. J. Neurosci. *27*, 9817–9823. https://doi.org/10.1523/JNEUROSCI.2707-07.2007.

40. Woodworth, H.L., Perez-Bonilla, P.A., Beekly, B.G., Lewis, T.J., and Leinninger, G.M. (2018). Identification of Neurotensin Receptor Expressing Cells in the Ventral Tegmental Area across the Lifespan. eneuro *5*, ENEURO.0191-17.2018. https://doi.org/10.1523/eneuro.0191-17.2018.

41. Takatoh, J., Park, J.H., Lu, J., Li, S., Thompson, P.M., Han, B.-X., Zhao, S., Kleinfeld, D., Friedman, B., and Wang, F. (2021). Constructing an adult orofacial premotor atlas in Allen mouse CCF. Elife *10*, e67291. https://doi.org/10.7554/eLife.67291.

42. Johns, D.C., Marx, R., Mains, R.E., O'Rourke, B., and Marbán, E. (1999). Inducible Genetic Suppression of Neuronal Excitability. J. Neurosci. *19*, 1691–1697. https://doi.org/10.1523/jneurosci.19-05-01691.1999.

43. Burrone, J., O'Byrne, M., and Murthy, V.N. (2002). Multiple forms of synaptic plasticity triggered by selective suppression of activity in individual neurons. Nature *420*, 414–418. https://doi.org/10.1038/nature01242.

44. Tucker, L.B., and Mccabe, J.T. (2017). Behavior of Male and Female C57BL/6J Mice Is More Consistent with Repeated Trials in the Elevated Zero Maze than in the Elevated Plus Maze. Front. Behav. Neurosci. *11*, 13. https://doi.org/10.3389/fnbeh.2017.00013.

45. Borsini, F., Podhorna, J., and Marazziti, D. (2002). Do animal models of anxiety predict anxiolytic-like effects of antidepressants? Psychopharmacology *163*, 121–141. https://doi.org/10.1007/s00213-002-1155-6.

46. Shaffer, F., and Ginsberg, J.P. (2017). An Overview of Heart Rate Variability Metrics and Norms. Front. Public Health *5*, 258. https://doi.org/10.3389/fpubh.2017.00258.

47. Kim, H.G., Cheon, E.J., Bai, D.S., Lee, Y.H., and Koo, B.H. (2018). Stress and Heart Rate Variability: A Meta-Analysis and Review of the Literature. Psychiatry Investig. *15*, 235–245. https://doi.org/10.30773/pi.2017.08.17.

48. Li, P., Janczewski, W.A., Yackle, K., Kam, K., Pagliardini, S., Krasnow, M.A., and Feldman, J.L. (2016). The peptidergic control circuit for sighing. Nature *530*, 293–297. https://doi.org/10.1038/nature16964.

49. Liu, S., Ye, M., Pao, G.M., Song, S.M., Jhang, J., Jiang, H., Kim, J.H., Kang, S.J., Kim, D.I., and Han, S. (2022). Divergent brainstem opioidergic pathways that coordinate breathing with pain and emotions. Neuron *110*, 857–873.e9. https://doi.org/10.1016/j.neuron.2021.11.029.

50. Yackle, K., Schwarz, L.A., Kam, K., Sorokin, J.M., Huguenard, J.R., Feldman, J.L., Luo, L., and Krasnow, M.A. (2017). Breathing control center neurons that promote arousal in mice. Science *355*, 1411–1415. https://doi.org/10.1126/science.aai7984.

51. Cohen, M.E., and White, P.D. (1947). STUDIES OF BREATHING, PULMONARY VENTILATION AND SUBJECTIVE AWARENESS OF SHORTNESS OF BREATH (DYSPNEA) IN NEUROCIRCULATORY ASTHENIA, EFFORT SYNDROME, ANXIETY NEUROSIS. J. Clin. Invest. *26*, 520–529. https://doi.org/10.1172/jci101836.

52. McGann, K.A., and Long, S.S. (2018). 21 - Respiratory Tract Symptom Complexes. In Principles and Practice of Pediatric Infectious Diseases, Fifth Edition, S.S. Long, C.G. Prober, and M. Fischer, eds. (Elsevier), pp. 164–172.e162. https://doi.org/10.1016/B978-0-323-40181-4.00021-9.

53. Kreibig, S.D. (2010). Autonomic nervous system activity in emotion: a review. Biol. Psychol. *84*, 394–421. https://doi.org/10.1016/j.biopsycho.2010.03.010.

54. Kim, S.-Y., Adhikari, A., Lee, S.Y., Marshel, J.H., Kim, C.K., Mallory, C.S., Lo, M., Pak, S., Mattis, J., Lim, B.K., et al. (2013). Diverging neural pathways assemble a behavioural state from separable features in anxiety. Nature *496*, 219–223. https://doi.org/10.1038/nature12018.

55. Daniel, S.E., and Rainnie, D.G. (2016). Stress Modulation of Opposing Circuits in the Bed Nucleus of the Stria Terminalis. Neuropsychopharmacology *41*, 103–125. https://doi.org/10.1038/npp.2015.178.

56. Wilson, T.D., Valdivia, S., Khan, A., Ahn, H.-S., Adke, A.P., Martinez Gonzalez, S., Sugimura, Y.K., and Carrasquillo, Y. (2019). Dual and Opposing Functions of the Central Amygdala in the Modulation of Pain. Cell Rep. *29*, 332–346.e5. https://doi.org/10.1016/j.celrep.2019.09.011.

57. Torres-Rodriguez, J.M., Wilson, T.D., Singh, S., Torruella-Suárez, M.L., Chaudhry, S., Adke, A.P., Becker, J.J., Neugebauer, B., Lin, J.L., Martinez Gonzalez, S., et al. (2024). The parabrachial to central amygdala pathway is critical to injury-induced pain sensitization in mice. Neuropsychopharmacology *49*, 508–520. https://doi.org/10.1038/s41386-023-01673-6.

58. Griessner, J., Pasieka, M., Böhm, V., Grössl, F., Kaczanowska, J., Pliota, P., Kargl, D., Werner, B., Kaouane, N., Strobelt, S., et al. (2021). Central amygdala circuit dynamics underlying the benzodiazepine anxiolytic effect. Mol. Psychiatr. *26*, 534–544. https://doi.org/10.1038/s41380-018-0310-3.

59. Boules, M., Li, Z., Smith, K., Fredrickson, P., and Richelson, E. (2013). Diverse roles of neurotensin agonists in the central nervous system. Front. Endocrinol. *4*, 36. https://doi.org/10.3389/fendo.2013.00036.

60. Kitabgi, P. (2002). Targeting neurotensin receptors with agonists and antagonists for therapeutic purposes. Curr. Opin. Drug Discov. Dev *5*, 764–776.

61. Slosky, L.M., Bai, Y., Toth, K., Ray, C., Rochelle, L.K., Badea, A., Chandrasekhar, R., Pogorelov, V.M., Abraham, D.M., Atluri, N., et al. (2020). beta-Arrestin-Biased Allosteric Modulator of NTSR1 Selectively Attenuates

Addictive Behaviors. Cell *181*, 1364–1379. https://doi.org/10.1016/j.cell.2020.04.053.

62. Tracy, L.M., Ioannou, L., Baker, K.S., Gibson, S.J., Georgiou-Karistianis, N., and Giummarra, M.J. (2016). Meta-analytic evidence for decreased heart rate variability in chronic pain implicating parasympathetic nervous system dysregulation. Pain *157*, 7–29. https://doi.org/10.1097/j.pain.0000000000000360.

63. Forte, G., Troisi, G., Pazzaglia, M., Pascalis, V.D., and Casagrande, M. (2022). Heart Rate Variability and Pain: A Systematic Review. Brain Sci. *12*, 153. https://doi.org/10.3390/brainsci12020153.

64. Wang, X., Zhang, Y., Wang, X., Dai, J., Hua, R., Zeng, S., and Li, H. (2020). Anxiety-related cell-type-specific neural circuits in the anterior-dorsal bed nucleus of the stria terminalis. Sci. Bull. *65*, 1203–1216. https://doi.org/10.1016/j.scib.2020.03.028.

65. Williford, K.M., Taylor, A., Melchior, J.R., Yoon, H.J., Sale, E., Negasi, M.D., Adank, D.N., Brown, J.A., Bedenbaugh, M.N., Luchsinger, J.R., et al. (2023). BNST PKCdelta neurons are activated by specific aversive conditions to promote anxiety-like behavior. Neuropsychopharmacology *48*, 1031–1041. https://doi.org/10.1038/s41386-023-01569-5.

66. Sakurai, K., Zhao, S., Takatoh, J., Rodriguez, E., Lu, J., Leavitt, A.D., Fu, M., Han, B.-X., and Wang, F. (2016). Capturing and Manipulating Activated Neuronal Ensembles with CANE Delineates a Hypothalamic Social-Fear Circuit. Neuron *92*, 739–753. https://doi.org/10.1016/j.neuron.2016.10.015.

67. Choi, H.M.T., Schwarzkopf, M., Fornace, M.E., Acharya, A., Artavanis, G., Stegmaier, J., Cunha, A., and Pierce, N.A. (2018). Third-generation in situ hybridization chain reaction: multiplexed, quantitative, sensitive, versatile, robust. Development *145*, dev165753. https://doi.org/10.1242/dev.165753.

68. Oh, S.W., Harris, J.A., Ng, L., Winslow, B., Cain, N., Mihalas, S., Wang, Q., Lau, C., Kuan, L., Henry, A.M., et al. (2014). A mesoscale connectome of the mouse brain. Nature *508*, 207–214. https://doi.org/10.1038/nature13186.

69. Chen, T.W., Wardill, T.J., Sun, Y., Pulver, S.R., Renninger, S.L., Baohan, A., Schreiter, E.R., Kerr, R.A., Orger, M.B., Jayaraman, V., et al. (2013). Ultrasensitive fluorescent proteins for imaging neuronal activity. Nature *499*, 295–300. https://doi.org/10.1038/nature12354.

70. Beier, K.T., Kim, C.K., Hoerbelt, P., Hung, L.W., Heifets, B.D., DeLoach, K.E., Mosca, T.J., Neuner, S., Deisseroth, K., Luo, L., and Malenka, R.C. (2017). Rabies screen reveals GPe control of cocaine-triggered plasticity. Nature *549*, 345–350. https://doi.org/10.1038/nature23888.

71. Yao, S., Wang, Q., Hirokawa, K.E., Ouellette, B., Ahmed, R., Bomben, J., Brouner, K., Casal, L., Caldejon, S., Cho, A., et al. (2023). A whole-brain monosynaptic input connectome to neuron classes in mouse visual cortex. Nat. Neurosci. *26*, 350–364. https://doi.org/10.1038/s41593-022-01219-x.

72. Reardon, T.R., Murray, A.J., Turi, G.F., Wirblich, C., Croce, K.R., Schnell, M.J., Jessell, T.M., and Losonczy, A. (2016). Rabies Virus CVS-N2c(DeltaG) Strain Enhances Retrograde Synaptic Transfer and Neuronal Viability. Neuron *89*, 711–724. https://doi.org/10.1016/j.neuron.2016.01.004.

73. Wang, X., Liu, Y., Li, X., Zhang, Z., Yang, H., Zhang, Y., Williams, P.R., Alwahab, N.S.A., Kapur, K., Yu, B., et al. (2017). Deconstruction of Corticospinal Circuits for Goal-Directed Motor Skills. Cell *171*, 440–455.e14. https://doi.org/10.1016/j.cell.2017.08.014.

74. Komada, M., Takao, K., and Miyakawa, T. (2008). Elevated plus maze for mice. J. Vis. Exp. *22*, 1088. https://doi.org/10.3791/1088.

75. López-Cano, M., Fernández-Dueñas, V., Llebaria, A., and Ciruela, F. (2017). Formalin Murine Model of Pain. Bio. Protoc. *7*, e2628. https://doi.org/10.21769/BioProtoc.2628.

76. Chaplan, S.R., Bach, F.W., Pogrel, J.W., Chung, J.M., and Yaksh, T.L. (1994). Quantitative assessment of tactile allodynia in the rat paw. J. Neurosci. Methods *53*, 55–63. https://doi.org/10.1016/0165-0270(94)90144-9.

77. Garrison, S.R., and Stucky, C.L. (2014). Contribution of transient receptor potential ankyrin 1 to chronic pain in aged mice with complete Freund's adjuvant-induced arthritis. Arthritis Rheumatol. *66*, 2380–2390. https://doi.org/10.1002/art.38724.

78. Tschida, K., Michael, V., Takatoh, J., Han, B.X., Zhao, S., Sakurai, K., Mooney, R., and Wang, F. (2019). A Specialized Neural Circuit Gates Social Vocalizations in the Mouse. Neuron *103*, 459–472.e4. https://doi.org/10.1016/j.neuron.2019.05.025.

79. Jennings, J.H., Sparta, D.R., Stamatakis, A.M., Ung, R.L., Pleil, K.E., Kash, T.L., and Stuber, G.D. (2013). Distinct extended amygdala circuits for divergent motivational states. Nature *496*, 224–228. https://doi.org/10.1038/nature12041.

80. Rodriguez, E., Sakurai, K., Xu, J., Chen, Y., Toda, K., Zhao, S., Han, B.-X., Ryu, D., Yin, H., Liedtke, W., and Wang, F. (2017). A craniofacial-specific monosynaptic circuit enables heightened affective pain. Nat. Neurosci. *20*, 1734–1743. https://doi.org/10.1038/s41593-017-0012-1.

81. Karey, E., Pan, S., Morris, A.N., Bruun, D.A., Lein, P.J., and Chen, C.-Y. (2019). The Use of Percent Change in RR Interval for Data Exclusion in Analyzing 24-h Time Domain Heart Rate Variability in Rodents. Front. Physiol. *10*, 693. https://doi.org/10.3389/fphys.2019.00693.

82. Mitchell, G.F., Jeron, A., and Koren, G. (1998). Measurement of heart rate and Q-T interval in the conscious mouse. Am. J. Physiol. *274*, H747–H751. https://doi.org/10.1152/ajpheart.1998.274.3.H747.

83. Janssen, P.M.L., Biesiadecki, B.J., Ziolo, M.T., and Davis, J.P. (2016). The Need for Speed: Mice, Men, and Myocardial Kinetic Reserve. Circ. Res. *119*, 418–421. https://doi.org/10.1161/circresaha.116.309126.

STAR★METHODS

KEY RESOURCES TABLE

REAGENT or RESOURCE	SOURCE	IDENTIFIER
Antibodies		
Goat anti-c-Fos pAb	Santa Cruz Biotechnology	Cat#sc-52-G; RRID:AB_2629503
Rabbit anti-c-Fos (9F6) mAb	Cell Signaling Technology	Cat#2250; RRID:AB_2247211
Rabbit anti-Neurotensin pAb	Immunostar	Cat#20072; RRID:AB_572254
Alexa Fluor 488 Donkey anti-Goat IgG	Jackson ImmunoResearch Labs	Cat#705-545-147; RRID:AB_2336933
Alexa Fluor 647 Donkey anti-Rabbit IgG	Jackson ImmunoResearch Labs	Cat#711-605-152; RRID:AB_2492288
Alexa Fluor 555 Donkey anti-Rabbit IgG	ThermoFisher Scientific	Cat#A-31572; RRID:AB_162543
Alexa Fluor 555 Donkey anti-Goat IgG	ThermoFisher Scientific	Cat#A-21432; RRID:AB_2535853
Bacterial and virus strains		
AAV2/1-EF1a-DIO-hChR2(H134R)-EYFP-WPRE	Karl Deisseroth	RRID:Addgene_20298
AAV2/8-CAG-FLEX-EGFP-WPRE	Oh et al.[68]	RRID:Addgene_51502
AAV2/8-CAG-FLEX-tdTomato	Edward Boyden	RRID:Addgene_28306
AAV2/1-hSyn-DIO-EGFP	Bryan Roth	RRID:Addgene_50457
AAV2/1-Syn-Flex-GCaMP6s-WPRE-SV40	Chen et al.[69]	RRID:Addgene_100845
AAV2/2-EF1a-DIO-eArch3.0-EYFP	UNC Vector Core	
AAV-hSyn-FLEX-loxP-Kir2.1-2A-GFP	Beier et al.[70]	RRID:Addgene_161574
AAV2/1-Syn-DIO-TVA66T-dTom-CVS-N2cG	Yao et al.[71]	RRID:Addgene_176285
RVdG(envA)-CVS-N2c-GFP	Neurotools	Reardon et al.[72]
AAV-CAG-FLEX-DTR	Harvard virus core	Wang et al.[73]
Chemicals, peptides, and recombinant proteins		
Phosphate buffered saline (PBS)	Thermo Fisher Scientific	Cat#10010023
Paraformaldehyde	Fisher Scientific	Cat#50-980-495
Tissue Tek O.C.T. Compound	Sakura Finetek	Cat#4583
Blocking One	Nacalai	Cat#03953-66
Dexdomitor (Dexmedetomidine)	Zoetis	
Ketamine Hydrochloride Injection	Dechra	
Formaldehyde solution	Millipore Sigma	Cat#252549
Complete Freund's Adjuvant	Millipore Sigma	Cat#F5881
4-hydroxytamoxifen	Millipore Sigma	Cat#H6278
Diphtheria Toxin	Millipore Sigma	Cat# D0564
Critical commercial assays		
Pdyn probe (HCR FISH)	Molecular Instruments	Custom Probe
Sst probe (HCR FISH)	Molecular Instruments	Custom Probe
Fos probe (HCR FISH)	Molecular Instruments	Custom Probe
Slc17a6 probe (HCR FISH)	Molecular Instruments	Custom Probe
Slc32a1 probe (HCR FISH)	Molecular Instruments	Custom Probe
Drd1 probe (HCR FISH)	Molecular Instruments	Custom Probe
Drd2 probe (HCR FISH)	Molecular Instruments	Custom Probe
Penk1 probe (HCR FISH)	Molecular Instruments	Custom Probe
Pkcd probe (HCR FISH)	Molecular Instruments	Custom Probe
Experimental models: Organisms/strains		
Fos[2A-iCreER] (TRAP2)	The Jackson Laboratory	RRID:IMSR_JAX:030323
NtsR1[ΔNEO−Cre]	The Jackson Laboratory	RRID:IMSR_JAX:033365

(Continued on next page)

Continued

REAGENT or RESOURCE	SOURCE	IDENTIFIER
Software and algorithms		
Prism 10	Graphpad	https://www.graphpad.com/features
Ponemah	Data Sciences International	
ANYmaze	Stoelting Co.	
Other		
Telemetric Sensors	Data Sciences International	Cat#ETA-F10
Optic fibers - photometry	RWD	Cat#BL400C-50NA
Optic fibers - optogenetics	RWD	Cat#BL200C-22NA
Patch fibers - photometry	Doric Lenses	Cat#MFP_400/430/1100–0.57_2m_FC-ZF1.25_LAF
Patch fibers - optogenetics	Doric Lenses	Cat#MFP_200/220/900–0.22_2m_FC-ZF1.25
Fiber photometry system	RWD	Cat #R821

EXPERIMENTAL MODEL AND STUDY PARTICIPANT DETAILS

All experiments were conducted following protocols approved by the Duke University and Massachusetts Institute of Technology (MIT) Institutional Animal Care and Use Committee. Adult (8–12 weeks) $Fos^{2A-iCreER}$ (TRAP2) mice (The Jackson Laboratory, strain #030323) and $NtsR1^{\Delta NEO-Cre}$ (The Jackson Laboratory, strain #033365) mice were used for experiments. Animals were housed in the vivarium with a 12-h light/dark schedule with *ad libitum* access to food and water.

METHOD DETAILS

Histology
Immunohistochemistry
Mice were transcardially perfused 90–120 min after exposure to a stimulus (anesthetic drug, diazepam, stress, pain) with phosphate buffered saline (PBS, pH 7.4, Thermo Fisher Scientific) followed by 4% paraformaldehyde (PFA). Brains were collected and post-fixed overnight at 4°C and then transferred to 30% sucrose solution and maintained at 4°C for 2 days. Brains were frozen in Tissue-Tek O.C.T. (Sakura) then cut into 80 μm thick sections on a cryostat (Leica). Sections were washed with PBS (3 × 5 min) then incubated in 1% Triton X-100 in PBS at room temperature for 2 h, blocked with 10% Blocking One (Nacalai Tesque) in 0.3% Triton X-100 in PBS at room temperature for 1 h, and then incubated at 4°C in primary antibody solution. The next day sections were washed (3 × 5 min in PBS) and incubated with species specific, minimally cross-reactive secondary antibody solution overnight at 4°C. Sections were again washed (3 × 5 min in PBS) and counter stained with 4′, 6-diamidino-2-phenylindole (DAPI, Sigma) and mounted with lab-made mounting media.[41]

Fluorescence **in situ** *hybridization*
Brains were prepared as described above and sectioned at 40–60 μm. To determine whether ovBNST_GA cells express prodynorphin (Pdyn) or somatostatin (Sst), fluorescence *in situ* hybridization was performed using Pdyn, Sst, and Fos probes.[18,66] Fluorescein iso-thiocyanate-labeled (FITC) Fos probe was used with digoxigenin-labeled (DIG) Pdyn or Sst probes to measure the co-localization with Fos in ovBNST_GA cells. To further examine the molecular identities of ovBNST_GA cells, HCR *in situ* hybridization was performed.[67] Briefly, all probes (Glut2, vGat, Drd1, Drd2, Penk1, Pkcd with Fos) were purchased from Molecular Instruments, hybridized with the sections overnight at 37°C, then amplified with the corresponding fluorescence-tagged (Alexa Fluor 488, 546 or 647) hairpins overnight at 25°C. Sections were washed, counter stained with DAPI, and mounted on day 3. Co-localization or overlap of each probe was measured against Fos in ovBNST_GA cells.

Imaging and quantification
Stained sections were imaged with a confocal laser scanning microscope (Zeiss LSM700). Cells were manually counted and quantified using ImageJ (NIH) to co-localize between: (1) *Fos* expressing neurons and neurons expressing the marker of interest and (2) isoflurane activated neurons and neurons activated by a different stimulus. Quantifications were performed by experimenters blinded to experimental conditions.

Drugs
Dexmedetomidine (Zoetis, 100 μg/kg), Ketamine (Dechra, 100 mg/kg), and Diazepam (MIT division of comparative medicine, 2 mg/kg (Fos), 3 mg/kg (telemetry)) were dissolved in sterile saline and injected intraperitoneally. Formalin (Sigma, 37% formaldehyde) was diluted to 4% in saline and injected unilaterally into the whisker pad (10 μL). Complete Freund's Adjuvant (CFA, Sigma, 1 mg/mL) injected bilaterally into the whisker pad (5 μL each side) or the plantar surface of the left hind paw (10 μL). Diphtheria toxin (50 μg/kg) was dissolved in saline and injected intramuscularly (i.m.).

IsoTRAP

TRAP2 mice express a tamoxifen-inducible, improved Cre-recombinase estrogen receptor fusion protein (iCreER) from the *Fos* promoter/enhancer elements.[23] To capture general anesthesia-activated neurons in the ovBNST, 2 weeks after stereotaxic deliveries of viruses, TRAP2 animals were anesthetized with 1.5% isoflurane mixed in 0.8 L/min oxygen for 1 h in a surgery induction chamber to induce the expression of FOS protein and iCreER. Briefly, 4-hydroxy tamoxifen was dissolved in pure ethanol through shaking at room temperature to make a 20 mg/mL solution. The solution was then mixed with corn oil and vacuum centrifuged to form a 10 mg/mL final solution of 4-hydroxy tamoxifen in corn oil. TRAP2 mice were intraperitoneally injected with 4-hydroxy tamoxifen at 50 mg/kg and put back in the induction chamber for 3 more h of isoflurane anesthesia.

Surgery

Stereotaxic viral injections

We used AAV2/1-EF1a-DIO-hChR2(H134R)-EYFP-WPRE, AAV2/8-CAG-FLEX-EGFP-WPRE,[68] AAV2/8-CAG-FLEX-tdTomato, AAV2/1-hSyn-DIO-EGFP, AAV2-EF1a-DIO-eArch3.0-EYFP, AAV2/1-Syn-Flex-GCaMP6s-WPRE-SV40,[69] AAV-hSyn-FLEX-loxP-Kir2.1-2A-GFP,[70] AAV2/1-Syn-DIO-TVA66T-dTom-CVS-N2cG,[71] RVdG(envA)-CVS-N2c-GFP,[72] and AAV-CAG-FLEX-DTR[73] for this study. To express desired genes in ovBNST neurons in Fos-TRAP2 or *Ntsr1*-Cre animals, mice were briefly anesthetized with isoflurane (3% isoflurane, 0.8L/min oxygen) before being transferred to a stereotaxic frame (David Kopf Instruments) with anesthesia maintained at 1.5% isoflurane mixed in 0.8L/min oxygen. Craniotomies were created with a dental drill (Aseptico) over the ovBNST, whose stereotaxic coordinates relative to bregma were: AP = +0.18 mm, ML = +/− 1.10 mm, DV = −3.65mm (DV coordinates relative to brain surface). The selected virus for the experiment was delivered using glass pipettes at a volume of 200–300 nL and a rate of 60 nL/min.

Optic fiber implant

For optogenetic activation and inhibition experiments, optic fibers (optogenetics: 200 μm core diameter, 0.22 NA; fiber photometry: 400 μm core, 0.5 NA; RWD) were implanted bilaterally over ovBNST with stereotaxic coordinates: AP = +0.18 mm, ML = +/− 2.23 mm, DV = −3.15 mm (relative to brain surface instead of skull surface) at 20-degree angles. Optic fibers were secured with Metabond (Parkell) and dental cement (Stoelting).

Telemetry sensor implant

Mice were anesthetized with 1.5% isoflurane mixed in 0.8L/min oxygen. The telemetric transmitters (ETA-F10; Data Sciences International) were implanted intraperitoneally. Briefly, two 1.5 cm midline incisions were made on the lower abdomen through the skin then through the abdominal wall. The transmitter was inserted into the abdominal cavity and secured to the muscle wall. The ECG electrode leads were tunneled through the muscle and under the skin to the right pectoral muscle (negative lead) and the left caudal rib region (positive lead). Muscle and skin openings were closed with sutures and animals were allowed 2 weeks for recovery.

Optogenetic activation and inhibition

Animals with optic fibers were connected to optical patch cables (0.22NA, 200 μm core diameter; Doric) coupled to a 473 nm (ChR2 activation) or a 561 nm (eArch3.0 inhibition) laser (Opto Engine LLC). Light pulses were generated with Ami-2 Optogenetic interface controlled by ANY-maze. The 473 nm laser was applied in pulses (~5 mW/mm^2, 20 Hz, 10 ms pulse width) in anxiety-like behavioral experiments and telemetry experiments and in continuous 5 s bins (~5 mW/mm^2) in telemetry experiments. The 561 nm laser was applied continuously (~10 mW/mm^2) to animals with eArch3.0 in anxiety-like behaviors.

Fiber photometry

Animals with optic fibers were connected to optical patch cables (0.57NA, 400 μm core diameter; Doric) coupled to a fiber photometry acquisition system (RWD R821). 470 nm and 410 nm light (~20–40 μW at fiber tip) was delivered through the patch cord. The resulting signal was collected through the same fiber and focused on a detector. Fluorescence was sampled at 90 fps. Mice were placed in a clear plastic cylinder with a small opening for the patch cord and tubing connected to a mobile isoflurane unit. For control oxygen trials, the recording started with a steady flow of 0.2% oxygen and 0% isoflurane. 5 min later, the oxygen was turned up to 0.8%, with isoflurane still at 0%. Recordings proceeded for another 5 min. For isoflurane trials, the recording started with a steady flow of 0.8% oxygen and 0% isoflurane. 5 min later, isoflurane was turned up to 2% and recordings proceeded for another 5 min. Each mouse received one oxygen and one isoflurane trial separated by at least 24 h.

Fiber photometry analysis

The 410 nm signal was used for motion and baseline correction. Z-scores were calculated using the standard deviation of the entire trace. Mean Z-scores were derived by calculating the average *Z* score and dividing by the integration time. Maximum Z-scores were calculated by identifying the highest *Z* score value for each mouse between times 0 and 60 s.

Behavioral assays

Open field test

To examine anxiety-like behaviors, mice were placed in a 30 * 30 * 30 cm plastic box with white floor and black walls. Each animal was initially placed in the center of the box. Locomotion activities were recorded with ANY-maze (Stoelting) through a webcam (Logitech) for a total of 10 min. Mice received 10 min of laser stimulation throughout the recording session, either 20 Hz pulses with the 473 nm

laser for ChR2 and control animals, or continuous light with the 561 nm laser for eArch3.0 and control animals. A 15 * 15 cm center zone was defined in ANY-maze tracking. Distance traveled and time spent in the whole apparatus and in the center zone were recorded and analyzed with ANY-maze.

Elevated plus maze test

To examine anxiety-like behaviors, mice were placed in an elevated plus maze for 10 min.[74] Locomotion activities were recorded with ANY-maze (Stoelting) through a webcam (Logitech). Mice received 10 min of laser stimulation throughout the recording session, either 20 Hz pulses with the 473 nm laser for ChR2 and control animals, or continuous light with the 561 nm laser for eArch3.0 and control animals. The open arms and closed arms were defined in ANY-maze tracking. Distance traveled and time spent in the whole apparatus, in the open arms, and in the closed arms were recorded and analyzed with ANY-maze.

Elevated zero maze test

To examine anxiety-like behaviors, mice were placed in an elevated zero maze for 10 min, which, compared to the elevated plus maze, removed the ambiguous and exposed center area between the open arms and closed arms.[44] Locomotion activities were recorded with ANY-maze (Stoelting) through a webcam (Logitech). Mice received 10 min of laser stimulation throughout the recording session, either 20 Hz pulses with the 473 nm laser for ChR2 and control animals, or continuous light with the 561 nm laser for eArch3.0 and control animals. The open arms and closed arms were defined in ANY-maze tracking. Distance traveled and time spent in the whole apparatus, in the open arms, and in the closed arms were recorded and analyzed with ANY-maze.

Conditioned place preference

Mice were allowed to freely explore a two-sided chamber for 20 min. The two sides were differentiated by the texture of the floor (ribbed vs. smooth) and by the wall pattern (white vs. striped). Animals were tracked using ANY-maze and the time spent in each side was recorded. During the next 4 days, animals were tethered to a patch cord coupled to a 473 nm laser and placed in their preferred side in the morning for 30 min without laser stimulation. In the afternoon, animals were again tethered and placed in their initially non-preferred side for 30 min and optogenetically stimulated as described above. On day 6, animals were again allowed to freely explore the arena for 20 min. The percent time spent in the stimulation-paired side (excluding time spent in the center) before and after conditioning was calculated for each mouse.

Stress

To induce stress, mice were placed in a Tailveiner restrainer (Braintree Scientific) for 90 min. For footshock stress, mice were exposed to 180 inescapable electric footshocks (0.4 mA) over a 30 min period. The duration of each shock was pseudo-randomized between 1 and 3 s and the inter-shock intervals were pseudo-randomized between 2 and 25 s.

Formalin assay

10 μL of 4% formalin (Sigma) was injected into either the left or right whisker pad of mice to induce acute pain. After the injection, mice displayed 2 distinct phases of self-recuperating behaviors (i.e., grooming/wiping of the injected area): the initial phase that lasted ~5 min due to acute peripheral pain; and the second phase that lasted more than 30 min due to ongoing inflammation and central sensitization.[75] The grooming/wiping/licking behavior of the injected whisker pad was video recorded immediately after formalin injection. To allow more time for manipulations, optogenetic stimulation was applied to mice at the start of the second phase in 2 min-ON 2 min-OFF cycles for 3 cycles (a total of 12 min, 6 min laser ON, 6 min laser OFF). Laser stimulation was given as 20 Hz pulses with the 473 nm laser for ChR2 and control animals, or continuous light with the 561 nm laser for eArch3.0 and control animals. The fraction of time spent displaying self-recuperating behaviors in each 2 min epoch was rated and calculated by an experimenter blinded to experimental conditions.

von Frey test

Mice were habituated for 2 h to individual plexiglass enclosures atop mesh flooring. On test days, mice were allowed to habituate for 1 h before testing began. To test the effects of ovBNST^{Ntsr1} activation on mechanical sensitivity, the up/down method[76] was used. For sham tests, mice were connected to the optic fiber without laser stimulation. For stim tests, 20Hz, 10ms stimulation was turned on during the test. Sham and stim tests occurred on the same day, with the order randomized across mice. At least 10 min separated sham and stim tests. To test the effect of chronic inactivation of ovBNST^{Ntsr1} neurons three von Frey filaments were applied (0.16g, 0.6g, and 1.4g) in ascending order. Force was applied until the filament bent. Each filament was applied 10 times to each paw, with at least 30 s in between trials. Withdrawals including lifting, shaking, or licking the paw were recorded, and the percent of trials after which a withdrawal was noted was calculated for each mouse and averaged across groups.

Hargreaves test

The same plexiglass and mesh flooring used for the von Frey test was used for the Hargreaves heat test. After a 1 h habituation, a guide light was used to position the infrared source directly under the left hind paw. The intensity was set to 30 and the reaction time was recorded. Withdrawals included lifting, shaking, or licking the paw. Each test included 3–5 trials, and the average was calculated and reported. Sham and stim tests occurred on the same day, with the order randomized across mice. At least 10 min separated sham and stim tests. Post-CFA heat and von Frey tests were performed on separate days.

Complete Freund's adjuvant (CFA)-induced persistent inflammation

A single administration of CFA has been reported to induce chronic inflammation pain in mice for over 2 weeks.[77] For whisker pad injections, two 5 μL injections of 1 mg/mL CFA (Sigma) were injected subcutaneously into the bilateral whisker pads. Swelling of injected whisker pads was observed hours after CFA injections. Anxiety-like behavioral tests were performed on day 3, 4, and 5 after

CFA injections. For paw injections, 10 μL was injected into the plantar surface of the left hind paw under brief isoflurane anesthesia. Sensory tests were conducted on days 1–3 after paw CFA injections.

Telemetry and breathing

Telemetric measurements

For 5 s stimulation experiments, mice were placed in an empty cage for 10 min, during which they received 5 s of continuous laser stimulation (~5 mW/mm^2 as described above) each minute. For 30 min stimulation experiments, mice were placed in an empty cage for 30 min where they received 20 Hz stimulation in a 3 min off, 3 min on paradigm. Heart rate and the beat-to-beat R-R intervals (RRI) were derived from ECG traces recorded and analyzed with the Ponemah software (Data Sciences International). Heart rate variability (HRV) was calculated as the square root of the mean squared differences between successive RR intervals (RMSSD).[46]

Breathing

Each mouse was head fixed to a custom elevated running disc setup using a headpost. Mice were tethered to optic fiber patch cables for the delivery of laser and a custom-built airflow sensor (AMW330V, Honeywell) was aligned to the snout of animals. Mice were allowed to habituate on the setup and were tested for 5 min. Mice received 5 s of continuous laser stimulation (~5 mW/mm^2, with 473 nm laser) during each 30 s trial (5 s of laser followed by 25 s of inter-laser interval). Respiratory activity was measured using an airflow sensor.[78] Voltage signals from the sensor were recorded at 250 kHz and down-sampled to 1kHz for analysis.

QUANTIFICATION AND STATISTICAL ANALYSIS

All statistical analyses were performed in GraphPad Prism 10. Significance levels were indicated as follows: *: $p < 0.05$, **:$p < 0.01$, ***: $p < 0.001$. Sample sizes were determined based on previous publications and common practice for comparable experiments.[18,54,79,80] Descriptive statistical results were presented as mean ± standard error.

Mice were randomly assigned to various treatment groups to receive viruses used for optogenetic manipulations and/or the various stimuli. Data recording and analysis was performed either automatically or by an individual blind to experimental conditions. Incorrectly virally targeted animals and invalid data entries were removed from the study. No sexual dimorphism in either histology or behavioral results was observed in the study, therefore results from males and females were grouped for analysis.

For behavioral experiments, 2-tailed paired or unpaired t tests and repeated measures two-way ANOVAs were used when appropriate with poshoc tests correcting for multiple comparisons (Holm-Šídák). Welch's correction or the Gessier-Greenhouse correction were used to account for unequal variance. Details on statistical tests and results can be found in Tables S1 and S2.

For telemetric measurements, heart rate, RRI and core body temperature measurements were outputted and logged at 1 Hz. Data entries were removed to exclude the possibility of abnormal consecutive heart beats or incorrect data logging where RRIs changed over 20% for 2 consecutive beats and were higher than 120 ms, as suggested by previous studies.[81,82] This manipulation also ensured basal heart rate data were within the normal range (~500–700 bpm) for conscious behaving mice.[83] Group data pooling all mice were used for plotting and statistical tests. Two-tailed t tests were performed to compare heart rate and RRI.